# Reactive Multidentate Block Copolymer Stabilization to Develop Thermoreversible Self-healable Hybrid Networks

Ge Zhang

A Thesis
in
The Department
of
Chemistry and Biochemistry

Presented in Partial Fulfillment of the Requirements
for the Degree of Master of Science (Chemistry) at
Concordia University
Montreal, Quebec, Canada

**July 2020**

# CONCORDIA UNIVERSITY

## School of Graduate Studies

This is to certify that the thesis prepared

By: Ge Zhang

Entitled: Reactive Multidentate Block Copolymer Stabilization to Develop Thermoreversible Self-healable Hybrid Networks

and submitted in partial fulfillment of the requirements for the degree of

**Master of Science (Chemistry)**

complied with the regulations of the University and meets the accepts standards with respect to originally and quality.

Signed by the final examining committee:

_____ Chair

Dr. Rafik Naccache

_____ Examiner

Dr. Zhibin Ye

_____ Examiner

Dr. Xavier Ottenwaelder

_____ Thesis Supervisor

Dr. John Oh

Approved by

_____

Dr. Yves Gélinas, Graduate Program Director

July.16.2020 _____

Dr. Pascale Sicotte, Dean of Faculty

# Abstract

## Reactive Multidentate Block Copolymer Stabilization to Develop Thermoreversible Self-healable Hybrid Networks

**Ge Zhang**

Self-healable crosslinked thermosets can prevent catastrophic failure and extend their lifetime due to their ability to recover the material properties after physical damages. A promising method to develop effective self-healable networks in repeating events is intrinsic self-healing that involves the utilization of mainly dynamic covalent linkages. Most of intrinsic self-healable networks have been designed with soft polymers to achieve rapid void-filling ability at low temperatures; however, they exhibit weak mechanical properties. The current and advanced development of intrinsic self-healable networks requires the balance of toughness and flexibility.

My Masters' thesis research has focused on the investigation of a new platform that allows for the development of heterogeneous thermoreversible networks. The platform centers on the exploration of reactive multidentate block copolymer (rMDBC) strategy to stabilize nanomaterials, particularly carbon nanotubes (CNTs). The rMDBC is designed with a pendant pyrene block that can bind to CNT surfaces through physical π-π interactions. A reactive furfuryl block can react with a polymaleimide to form thermally-reversible networks through dynamic Diels-Alder (DA)/retro-DA (rDA) chemistry. The formed rMDBC/CNT colloids are acted as multiple crosslinkers for macromolecular engineering approach to form a robust heterogeneous network in which CNTs are covalently integrated, thus leading to uniform distribution of CNTs in self-healable networks. Taking advantage of characteristics of polyurethane (PU) including shape memory and hydrogen bonding, the developed materials exhibit robust self-healability and potentially enhanced mechanical property and conductivity.

# Acknowledgement

I would like to thank my supervisor, Dr. John Oh, for giving me the valuable opportunity to build up my academic career. He contributed big amount of time to support my scientific research, manuscript preparation, and thesis writing. The completion of this project could not be accomplished without the support of him. I would like to emphasize my deepest gratitude to his professional training and education during all my master study. As my supervisor and mentor, what Dr. John Oh taught me does not only the knowledge of polymer science, but also the ways to overcome the difficulties during research process, even life.

I also would like to thank my committee members Dr. Zhibin Ye and Dr. Xavier Ottenwaelder for their academic support. Their valuable suggestions and helpful comments always inspire me to optimize my research. I really appreciate it that they are always generous to provide academic support whenever I ask for a favor.

It is my honor that I have spent a great time with all my colleagues, especially Arman and Twinkal, from OH group. They shared their knowledge with me and even provided effective suggestions when I was faced with dilemmas of research. Their continuous support and great friendship delight my research life.

The encouragement and love from my dear families and friends are incredibly supportive throughout all the entire process. I would like to especially thank my parents, my grandparents and my boyfriend with my deepest gratitude for what they dedicated in all aspects for me.

# Contribution of Authors

All the research presented in this thesis was conducted independently by the author under the supervision of Dr. Oh at Concordia University. 3-Phenylpropyl 2-bromo-2-methylpropanoate was synthesized by Dr. Jung (former Postdoc in Dr. Oh's laboratory) and viscoelastic property measurements of dried matrix via using rheometer were conducted with aids of Twinkal Patel (PhD student in the Dr. Oh's laboratory).

# Table of Contents

# List of Figures

# List of Abbreviation

| | |
|---|---|
| rMDBC | Reactive multidentate block copolymer |
| CNTs | Carbon nanotubes |
| ATRP | Atom transfer radical polymerization |
| FRP | Free radical polymerization |
| CRP | Controlled radical polymerization |
| DP | Degree of polymerization |
| $M_n$ | Number average molecular weight |
| $M_w$ | Weight average molecular weight |
| PDI | Polydispersity |
| DA | Diels-Alder |
| CuBr | Copper (I) bromide |
| $^1$H-NMR | Proton nuclear magnetic resonance |
| $^{13}$C-NMR | Carbon nuclear magnetic resonance |
| GPC | Gel permeation chromatography |
| TGA | Thermal gravimetry analysis |
| DSC | Differential scanning calorimetry |
| UV-vis | Ultraviolet-visible |
| FT-IR | Fourier transform infrared spectroscopy |
| AFM | Atomic force microscopy |
| HRMS | High resolution mass spectrometry |
| TLC | Thin-layer chromatography |
| $CDCl_3$ | Deuterated chloroform |
| THF | Tetrahydrofuran |
| DCM | Dichloromethane |
| EA | Ethyl acetate |
| HE | Hexane |
| DMF | Dimethylformamide |
| BM | 1,1'-(methylenedi-4,1-phenylene) bismaleimide |
| $Et_3N$ | Triethylamine |
| HEMA | 2-hydroxylethyl methacrylate |
| LiBr | Lithium bromide |
| $Na_2SO_4$ | Sodium Sulfate |
| $T_g$ | Glass transition temperature |
| Br-iBuBr | α-bromoisobutyryl bromide |
| FuMA | Furfuryl methacrylate |
| Py-OH | 1-pyrenemethanol |
| CDI | 1,1′-Carbonyldiimidazole |
| CDI-MA | 1,1′-Carbonyldiimidazole methacrylate |
| PyMA | Pyrene methacrylate |
| DMAP | 4-dimethylamino pyridine |
| PMDETA | N,N,N′,N″,N″-Pentamethyldiethylenetriamine |
| OH-PCL-OH | Polycaprolactone diol |
| MDI | 4,4′-Methylenebis(phenyl isocyanate) |
| DBTDL | Dibutyltin dilaurate |
| Fu-OH | Furfuryl alcohol |

# Chapter 1
# Literature review and thesis scope

## 1.1 Recent strategies to fabricate self-healable crosslinked networks

### 1.1.1 Introduction

Popular artificial materials nowadays, have been effectively designed utilizing polymers with multifunctionalities for wide applications in the fields of nanoscience, biotechnology, and materials science. However, the formation of inevitable microcracks decrease their work efficiency and cause catastrophic failures, in the materials. In early 1980, the concept of self-healing polymeric materials was proposed to be capable of healing invisible microcracks.[1, 2] Benifiting from crosslinked thermosets, self-healing polymeric network materials exhibit high-performance in mechanical properties and thermal stability.[3] Smart materials are able to repair damages and cracks automatically (with no stimuli)[4] or in respond to external stimuli.[5, 6] The emergence of polymeric materials have significantly extended their lifetime and broaden their applications. Due to these features, a variety of self-healing strategies have been developed, which can be classified into two systems: intrinsic and extrinsic.

Intrinsic self-healing system consists of reversible (or dynamic) crosslinks such as reversible covalent bonds or supramolecular (physical) associations. Figure 1.1 illustrates typical reversible linkages reported in literature for the development of novel self-healable materials.[7] Many of the intrinsic self-healing systems are triggered by light,[8] pH,[9] electrical field,[10] moisture[11] or temperature.[12] However, others require no stimuli to initiate self-healing.[13] Upon mechanical damages and cracks, the dynamic linkages will be cleaved, followed bypolymer chains to flow and fill the formed voids (called void-filling). The dynamic linkages can recombine in response to external stimuli, allowing such dissociation and recombination to attain self-healing and retain mechanical properties. In such, well-designed intrinsic systems allows for multi healing events, which is considered an advantage compared to extrinsic systems.[14]


**Figure 1.1** An illustration of typical reversible linkages reported in literature for the development of novel self-healable materials.[7]

Extrinsic self-healing systems involve the encapsulation of external healing agents such as monomers, catalysts, or crosslinkers[15]in the forms of microcapsules[16] or vascular networks,[17] which are dispersed in polymer matrices. Physical cracks or damages could trigger the release of healing agents which would fill and repair the damaged parts by polymerization or chemical reactions. As a consequence, the systems can heal large damaged areas, but a disadvantage being it allows only a single event of healing due to the consumption of external healing agents.

Despite these advances, the limitation of mechanical strength and thermal properties restricts further applications of self-healable networks based on only polymers in industries.[18-20] To solve this problem, an incorporation of hard additives in the design of self-healable networks has been extensively explored. [21] Further, it is highly desirable to develop novel self-healing networks that maintain integrity and mechanical properties.

### 1.1.2 Intrinsic self-healing systems through reversible chemical crosslinking methods

These materials achieve damage repairing though inherent reversibility of covalent bonds in polymer matrices. Chemical bonds can reform on damaged areas under appropriate stimulus (pH, light, temperature, or oxygen)[6, 22] and generally they provide higher mechanical strength compared to non-covalent interactions. A range of self-healing networks are described in this section, based on disulfide bonds, Diels-Alder reactions and hinder urea bonds, etc.

#### 1.1.2.1 Disulfide chemistry

Disulfide bond is a dynamic covalent bond that can be cleaved to its corresponding thiols or thiyl radicals in response to pH, reducing agent, mechanical energy, or light.[23] They then react to reform disulfide bonds via oxidation, thiol-disulfide exchange reaction, or combination of thiyl radicals.

Matyjaszewskii's group has reported a strategy to develop novel self-healing polymeric materials based on disulfide bonds in 2012. Their grafted star polymers with disulfide reversible linkages at branch peripheries were synthesized via a tom transfer radical polymerization (ATRP). Disulfide bonds were cleaved under reducing condition to form thiol-functionalized star polymers, which reformed disulfide crosslinked networks via oxidation. The multiarmed polymers containing disulfide bonds shows effective self-healability due to low intrinsic viscosity and high accessibility of functional groups.[24]

Zhao group designed self-healing superamphiphobic coatings, where disulfide bonds are integrated in polyurethane (PU) to achieve healing of cracks via disulfide exchange reaction under UV light irradiation. Disulfide-containing PU was synthesized with several small molecules through polyaddition. UV light stimulated the polymer chain re-organized through thiol-disulfide exchange reaction.[25]

Oh research group reported a novel dual sulfide-disulfide crosslinked networks fabricated by a combination of photo-induced thiol-ene click-type radical addition, generating lightly sulfide-crosslinked polysulfide-based networks with excess thiols, and their oxidation, creating dynamic disulfide crosslinks. The formed networks exhibit rapid and room temperature self-healability within seconds to minutes, with no extra healing agents or change in environmental conditions.[26] Later, the group reported a new multiblock copolymer self-healing strategy that centers on the

synthesis of block copolymers designed with different self-healing motifs incorporated into individual blocks. As illustrated in Figure 1.2, the copolymer was fabricated to multifunctional materials self-healable on macro-scale damages through supramolecular metal-ligand interactions and disulfide exchange reactions at room or moderate temperatures.[27]

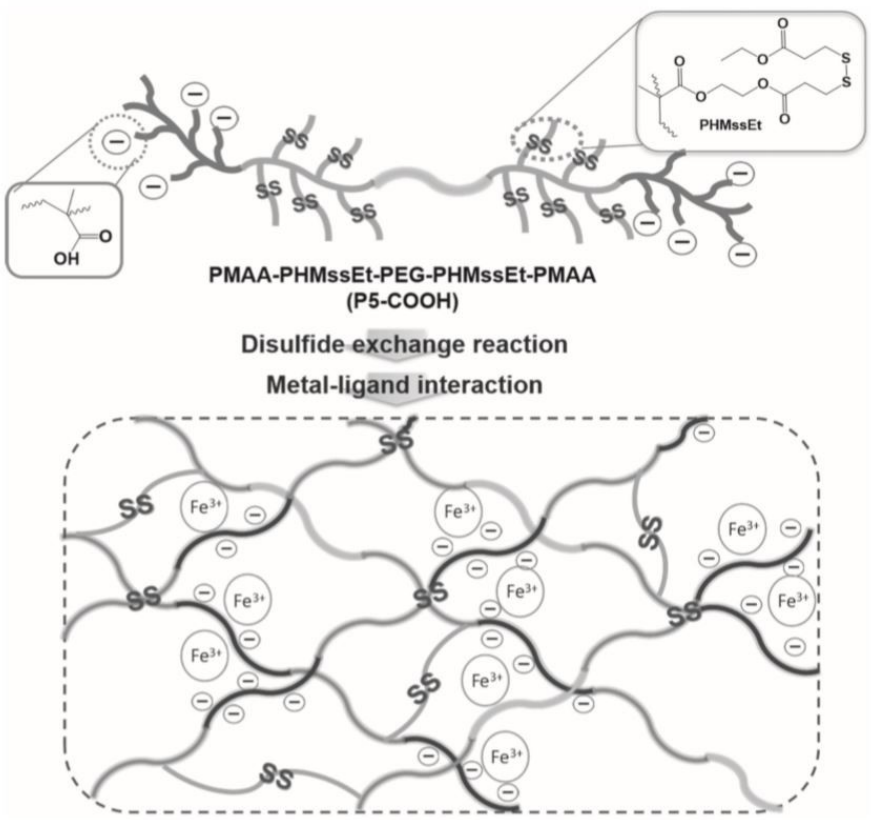


**Figure 1.2** Illustration of the approach to prepare dual crosslinked networks based on a novel pentablock copolymer exhibiting dual self-healing through covalent disulfide exchange reaction and supramolecular metal-ligand interaction.[27]

### 1.1.2.2 Diels-Alder (DA)/retro-DA chemistry

Compared to other stimuli in intrinsic self-healing systems such as light, pH, electrical field or moisture, temperature stimulus has been investigated widely due to its relatively practical applications. In particular, Diels-Alder(DA) reaction, which is a [4+2] cycloaddition of a diene and a dienophile.[28], received special attention from many academics. Furan groups and maleimide groups have been used most often as typical diene and dienophile respectively, because they can proceed in the absence of catalyst without any side reactions and by-products. At elevated temperature (>120 °C), the formed cycloadducts resulted from DA reactions are

dissociated to the corresponding furan and maleimide moieties through retro-DA (rDA) reaction. Upon cooling down, they are recombined to DA adducts through DA reaction. Such dynamic DA/rDA chemistry plays a significant role in achieving high healing efficiency of thermoreversible self-healing materials.

Considering the architectures of self-healing polymers via DA chemistry, various synthetic strategies have been explored. The strategy involves cycloaddition reaction of polyfurans and polymaleimides, yielding linear thermoplastic and crosslinked thermoset polymers.[29] Berto et al reported the synthesis of furan telechelic 1,4-cis-polydienes, which were used for polyaddition with bismaleimide (a dimaleimide), leading to the formation of a reversible network via DA chemsitry.[30]

Oh research group has also developed several novel strategies to synthesize thermally-labile networks crosslinked with DA-induced cycloadducts. The strategies center around the thermoreversible networks based on methacrylate copolymers bearing either furan[31] or maleimide pendants[32-34] that were synthesized by ATRP technique. Polymethacrylate backbones consist of carbon-carbon single bonds, high molecular weight of polymeric chains, and facile copolymerization with soft monomers allow for tuning a balance between rigidity and flexibility of methacrylate networks. Furthermore, the group reported a new approach based on macromolecular engineering through thermoreversibility to fabricate the engineered gel networks of thermally-labile branched polymers exhibiting robust self-healing. As illustrated in Figure 1.3, the formed networks exhibit effective self-healing, demonstrated with reconstruction of two separate pieces and complete void-filling on surface cuts as well as recovery of healing viscoelasticity.[29]

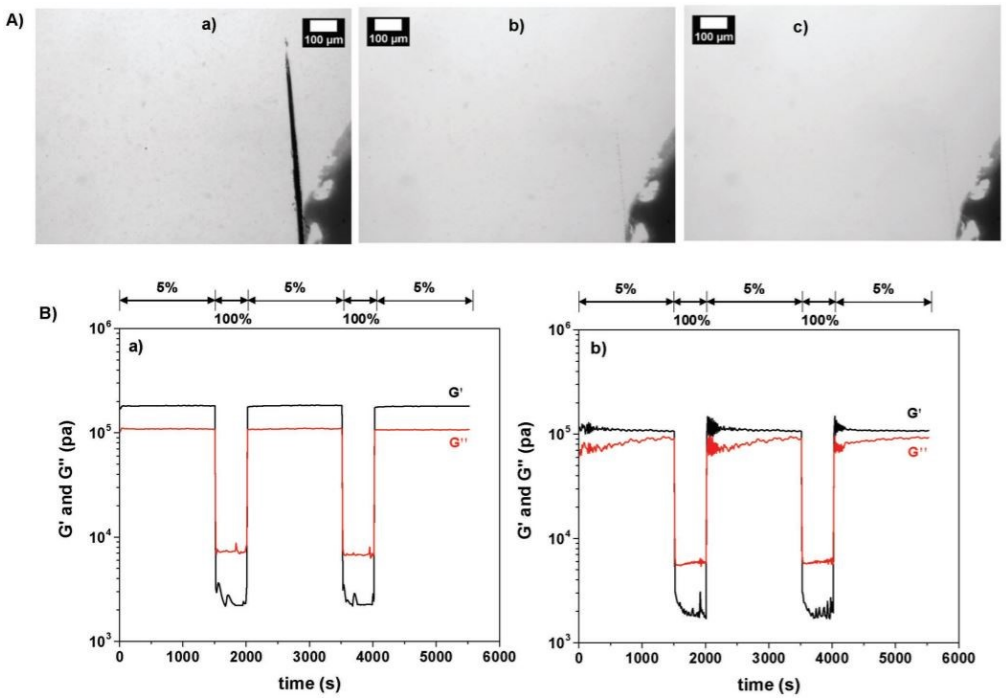


**Figure 1.3** A) Optical microscope images with a micrometer-sized cut on surface of gels before (a) and after healing at 120 ℃ for 10 (b) and 30 (c) mins as well as B) their viscoelastic properties upon a cyclic change of oscillation force: 5% stain for 1500 s to 100% strain for 500 s before (a) and after (b) healing at 10 min.[29]

### 1.1.2.3 Other reversible chemistries

Hindered urea bonds have been utilized for self-healing based on their dissociation into isocyanate and amine reversibly. They respond to a variety of chemical signals, such as amine, alcohol, water, hydrogen peroxide.[35] Recently, the development of catalyst-free, ambient-temperature and hydrolysable polymers containing hindered urea bonds were reported.[36]

Imine bonds are strong covalent bonds with a bond dissociation energy of 147 kcal/mol, providing promising mechanical properties . They can involve rapid degenerative bond exchange without any significant side reactions.[37] Recent report describes the combination of poly(ethylene glycol) with imine bonds to be an attractive strategy to develop self-healing hydrogels.[38] In addition, acylhydrazone,[39] olefin metathesis,[40] boronic ester,[41] and coumarin dimer[42] chemistries have also been explored for intrinsic self-healing networks.

### 1.1.3 Intrinsic self-healing systems through supramolecular associations

Dynamic networks through of non-covalent (physical) interactions have been designed through hydrogen bonding and metal complexation as well as π-π, ionic, and host-guest interactions.[43] The formed physical crosslinks are dissociated in response to stimuli, including pH, temperature, and mechanical stress. They are restored to their original interactions due to the reversibility of the physical crosslinks.

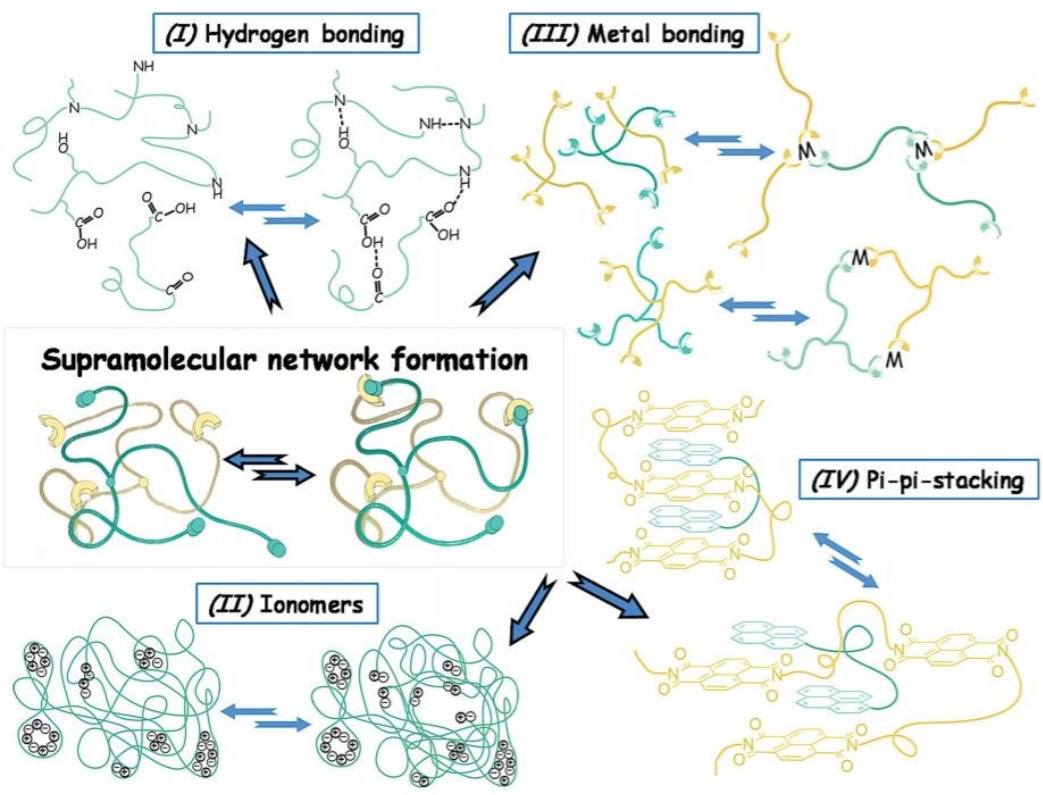


**Figure 1.4** Supramolecular network formation via (i) hydrogen bonding, (ii) ionomers (iii) metal bonding, and (iv) π-π stacking.[43]

#### 1.1.3.1 Hydrogen bonding

As one of most well-established supramolecular associations, hydrogen bonding plays a significant role in the development of self-healing networks. The strategy involves the incorporation of hydrogen bonding motifs as donors and acceptors into polymers backbones, pendants, or terminal groups. Various hydrogen bonding motifs have been applied and 2-ureido-4-pyrimidone moieties,[44] carboxylic acid groups,[45] hydroxyl groups,[46] urea moieties,[47] and amide groups[48] are typical examples. Due to intermolecular interactions via hydrogen bonds, the

designed polymers possess reversible supramolecular crosslinking networks. They can reform the supramolecular networks autonomously after physical damages. Further research is focusing on the improvement of the weak mechanical properties of hydrogen bonding networks, and a promising strategy is proposed to incorporate hard domains, such as inorganic nanomaterials and hard segment of polymer chains.[49]

#### 1.1.3.2 π-π interactions

π-π interaction forms among aromatic units. The two residues, π-electron-rich and π-electron-deficient residues, induce chain folding via π-π stacking under thermal stimulus.[50] Justin et al reported a healable supramolecular polymer blend that consists of π-electron rich pyrenyl terminated oligomer and another oligomer with π-electron poor naphthalene-diimide units. The formed supramolecular nanocomposite containing cellulose nanocrystal shows the healing efficiency to be as high as 90% recover from the original tensile modulus.[51]

#### 1.1.3.3 Ionic interactions

Ionic crosslinking networks for self-healing involves mutual interactions of anionic polymers with cationic species. They can break under physical rupture and subsequently re-interact in response to external stimulus such as temperature or ultraviolet irradiation.[52] Lapitsky et al reported self-healing hydrogels, fabricated by mixture of cationic poly(allylamine) and anionic pyrophosphate or tripolyphosphate.[53] Also, ferric ions were utilized to form dynamic ionic interactions with carboxylic groups of poly(acrylic acid).[54, 55] Due to the electrostatic interactions between cations and anions, the materials possess self-healability and conductivity simultaneously.[56]

#### 1.1.3.4 Host-guest interactions

Host-guest interactions is one of the most important non-covalent interactions for the development of intrinsic self-healing systems. The interactions usually involve multiple reversible non-covalent interactions, such as hydrogen bonds, electrostatic interactions, van der Waals forces, etc. Binding affinity between the host and guest molecules strongly affect the self-healability of materials.[57] Typical host– guest chemistries include cyclodextrins, sulfonatocalixarenes, and cucurbiturils.[58] As reported by Hu et al, intrinsic self-healing epoxy

resis were fabricated based on host-guest interactions between β-cyclodextrin and azobenzene, and self-healing was triggered by heat or photothermal via graphene as fillers.[59]

#### 1.1.3.5 Metallo-supramolecular interactions

Metallo-supramolecular interactions happen between polymeric ligands and metal ions, such as Zn, Fe, Co, and Ni.[60] The interactions can be disrupted by response to physical, thermal, or UV stimulus, and their restoration can induce self-healing behavior. Typically, Qifeng et al reported the development of a self-healing nanocomposite crosslinked through metallo-supramolecular associations of terpyridine-terminated polyurethane with $Zn^{2+}$ ions.[61]

### 1.1.4 Extrinsic self-healing systems

In contrast to intrinsic self-healing methods, which achieve self-healing via reversibility of chemical bonds or physical interactions, extrinsic self-healing methods require the encapsulation of external healing agents in various forms of containers, such as microcapsules, microfibers, and vasculatures. When the containers are ruptured through the development of cracks in the thermoset composites, the healing agents are released to repair the damages through polymerizations or chemical reactions. However, the consumption of localized healing agents results in one-off healing event in the damaged regions.[15, 20]

Microcapsule-based extrinsic self-healing system, are of particular interest, as healing agents encapsulated in discrete microcapsules are sequestered in self-healing matrices. The damages trigger the rupturing of the microcapsules from which the content is released. Common encapsulation techniques applied in self-healing materials are in-situ, interfacial, and melt dispersions.[62] Their design cycle consists of five steps generally: development, integration, mechanical characterization, triggering, and healing damage.[63] The important parameters that have to be considered in the design and synthesis of microcapsules include capsule sizes, uniform dispersion of capsules, mechanical properties, and miscibility of shells with matrices. White et al reported the encapsulation of a healing agent in microcapsules while monomers and catalysts are dispersed in matrix. Healing process was achieved by ring opening metathesis polymerization of dicyclopentadiene in the presence of Grubbs' catalyst.[64] Keller et al reported the exploration of a platinum-catalyzed hydrosilylation of vinyl-terminated dimethylsiloxane resin, in which healing agents and monomers were encapsulated in microcapsules.[65] Further to aid in chain growth polymerization techniques, reports describe the exploration of facile organic

reactions as another healing mechanism. For this mechanism, the polymers should bear reactive functionality in matrices that can react with healing agents released from confined microcapsules. Caruso et al reported the use of residual amine functionality in an epoxy matrix.[66]

### 1.2 Surface modification of carbon nanotubes (CNTs)

Due to sp2 hybridized carbon-carbon bonds, CNTs show excellent mechanical properties[67] and high electrical conductivity.[68] They possess theoretical and experimental Young's modulus of as high as 1.2 TPa and tensile strength of 50 – 200 GPa.[69] CNTs have conductivity of 2000~6000 W/mK at room temperature.[70]

In order to expand and refine applications of polymeric materials, CNTs have been considered as promising nanomaterials to improve their mechanical and conductive properties. However, there are difficulties in dispersing bare CNTs homogeneously as reinforcement additives into polymer matrix, which severely limits properties of the composites. Various dispersion techniques such as ultrasonication and mechanical stirring have been explored to reduce intermolecular forces among CNTs and thus the size of agglomeration.[71] While these techniques reconfigure a new equilibrium state to reform aggregation, they often result in the inhomogeneous dispersion of CNTs in polymer matrix.[72] The brief review below focuses on the studies that develop stabilization/functionalization techniques of the interfacial interaction enhancement between CNTs and polymers, to avoid the inherent entanglement. There are two stabilization categories based on different interacting strategies with polymers, covalent chemical bonding (chemical modification) and non-covalent interaction (physical modification).

#### 1.2.1 Chemical modification

Chemical modification involves the attachment of surface ligands to CNT surfaces through covalent bonds. This method have been achieved by the reaction between CNTs and some molecules with high reactivity, such as fluorine.[73, 74] Other reactions of direct sidewall functionalization, including cycloaddition,[75] hydrogenation,[76] and radical attachment[77] also have been investigated successfully. Defect functionalization is another method to achieve covalent modification, which takes advantage of defect sites on CNTs, for example, open ends, holes and oxygenated sites. Defect sites can be created on CNTs by oxidizing reaction with strong acid or strong oxidants.[78] Due to stabilization with carboxylic acid or hydroxyl groups on the defects,

these functionalized CNTs can be used as precursors for further reactions, such as silanization,[79] polymer grafting via living polymerization.[80]

### 1.2.2 Physical modification

Considering the strict reaction requirements for CNTs functionalization based on covalent bonds, it is necessary to put efforts on the development of alterative methods. Meanwhile, the method maintaining the original framework of CNTs also attracts attention, because non-covalent functionalization, involving physical adsorbing or wrapping, possibly maintains its conductivity and mechanical properties. As one of widely applied non-covalent methods, polymer wrapping happens between CNTs and polymers containing aromatic moieties via van der Waals force or π-π stacking. CNTs were stabilized with conjugated polymers such as poly(phenylene vinylene), polypyrene, and polystyrene.[81] Adsorption surfactant, including non-ionic, anionic, cationic surfactants, has also been utilized for CNTs modification.[82] Due to surfactant reducing the surface tension of CNTs, it is an effective method to prevent aggregations of CNTs. CNTs also can be functionalized via endohedral method which is based on the capillary effect. It is not a wise option to avoid re-agglomeration of CNTs, while it is utilized as catalysis, energy storage and so on.[83]

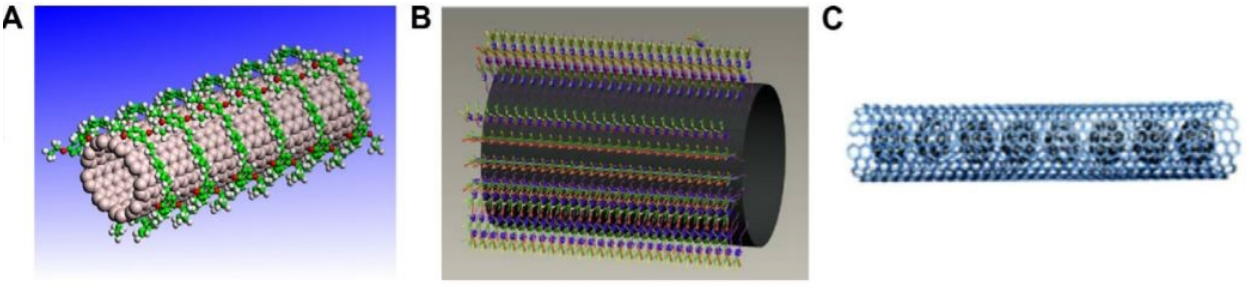


**Figure 1.5** Schematics of CNTs functionalization using non-covalent methods: A) polymer wrapping, B) surfactant adsorption, and C) endohedral method.[84]

## 1.3 Polyurethane (PUs)

Polyurethanes (PUs) are generally prepared by step-growth polymerization through polyaddition of polyisocyanates and polyols. Their chemical structures and compositions can be tuned with the choice of reactants. This can make PUs to be considered as versatile materials with great potential for various applications. Thermoplastic PUs are widely used for mobile

electronic devices.[85] Flexible PUs are usually applied as cushion materials in furniture, bedding, and biomedicine.[86] Rigid PU foams are promising insulation materials[87] while PU ionomers are used for biomaterials.[88]

PUs possess low density, chemical inertness, low cost, and versatile frication methods. Due to these advantages, PUs have been explored as an ideal polymer matrix in the development of self-healing materials in recently years, especially combining with Diels-Alder chemsitry.[89-93] In the work of Guadalupe Rivero, DA adducts (furan and maleimide moieties) were introduced as crosslinkers into polycaprolactone-based PU networks. Polycaprolactone was used to provide PUs with shape memory property that favors the crack closure under thermo-stimulus and improves the mechanical properties.[49] PU materials also were formulated with dynamic disulfide bonds to achieve self-healing.[94]

## 1.4 Scope of the thesis

My MSc thesis consists of four chapters to describe our efforts in exploring a new platform that develop heterogeneous thermoreversible networks to which CNTs are covalently embedded through reactive multidentate block copolymer (rMDBC) strategy, exhibiting robust self-healability and uniform distribution. Chapter 1 discusses fundamentals and mapping out recent advances in the development of self-healable systems, Chapter 2 presents our published results on reactive multidentate block copolymer stabilization to CNTs for thermoreversible crosslinked network gels. Our work on macromolecularly-engineered thermoreversible heterogeneous self-healable networks encapsulating reactive multidentate block copolymer-stabilized carbon nanotubes is summarized in Chapter 3. Finally, Chapter 4 concludes our works and present future directions to improve our platform.

# Chapter 2

# Reactive multidentate block copolymer stabilization to carbon nanotubes for thermoreversible crosslinked network gels

This chapter is reproduced the article published in *ACS Applied Polymer Materials,* **2020**, *2,* 2319-2326 with permission from the publisher.

## 2.1 Introduction

Colloidal carbon-based and inorganic nanomaterials have been a promising choice of key components in the construction of multifunctional (nano)materials for various applications in nanotechnology, biotechnology, materials science, electronics, and solar cells.[95-101] This is because these nanomaterials possess their distinct properties - conductivity, emission, upconversion, magnetization, antimicrobial, etc. To maximize their excellent properties as well as to ensure their compatibility with application environments, the control over their surface chemistry is essential.[102, 103] Small molecules and oligomers having one or two anchoring groups have been extensively used; however, the resultant nanomaterials stabilized with such monodentate or bidentate ligands tend to be aggregated because of physical equilibrium of adsorption/desorption of anchoring groups on the nanomaterial surfaces. In contrast, polymers are considered as multidentates possessing multiple anchoring groups that bind to the surfaces of the nanomaterials[102] and even enzymes.[104, 105] Compared with homopolymers and biopolymers,[106, 107] multidentate block copolymers (MDBCs) have stronger binding ability due to more favourable conformational arrangements of multiple anchoring groups tethered from a long polymeric block onto surfaces. Further to the binding block having pendant anchoring groups, the MDBCs are designed with the other block that endows compatibility with environments. For example, the versatility of MDBC stabilization strategy has been demonstrated to fabricate aqueous colloids of superparamagnetic iron oxide nanoparticles (SNPs) stabilized with a block copolymer consisting pendant either carboxylic acid or catechol groups in one block and pendant oligo(ethylene oxide) groups in the other block.[108-110] The formed colloids at single layers exhibit enhanced colloidal stability as well as magnetic properties. Furthermore, the enhancement of

luminescent and magnetic properties for aqueous colloids of quantum dots[111, 112] and zinc oxide nanoparticles[113] through MDBC stabilization strategy has been reported.

Given these benefits of MDBC stabilization strategy, we have envisioned that the design and synthesis of reactive MDBCs (rMDBCs) can be an effective platform in the development of high performance, dynamically-crosslinked materials. Compared with conventional MDBCs with a compatible block, rMDBCs consist of a reactive block with pendant functional groups along with a anchoring block. The formed rMDBC/nanomaterial colloids can act as multiple crosslinkers that enable the integration of the nanomaterials covalently in reversibly-crosslinked composites and coatings. This rMDBC strategy can be anticipated to ensure the uniform distribution of nanomaterials in covalent adaptable networks (CANs) through the formation of dynamic (or reversible) crosslinks.[114-116] The formed heterogeneous CANs can provide improved mechanical and nanomaterial-intrinsic properties.

In this work, we have explored new rMDBC stabilization strategy with the synthesis of a novel rMDBC having pendant furfuryl groups in one block and pyrene groups in the other block. The furfuryl groups are designed to react with maleimide groups in polymaleimides through Diels-Alder (DA) reaction to form thermally-labile crosslinked networks,[28, 117-119] while the pyrene groups physically anchor to the surface of carbon materials through π-π interactions.[120-122] As a proof-of-concept, multi-walled carbon nanotubes (CNTs) were chosen as a model nanomaterial to investigate our rMDBC stabilization strategy. CNTs possess outstanding electrical, optical, and thermal properties.[123-126] As illustrated in Figure 2.1, the rMDBC enabled the stabilization of CNT surfaces to form colloidally-stable rMDBC/CNT colloids. For comparison, a homopolymer bearing pendant pyrene groups (MDHP) and a monodentate homopolymer bearing a pyrene terminal group (MoDHP) were synthesized to demonstrate the versatility of rMDBC stabilization to CNT surfaces. Further, the applicability of the formed rMDBC/CNT colloids bearing multiple furfuryl groups as reactive crosslinkers was investigated toward to fabrication of dynamic crosslinked network gels exhibiting thermoreversibility through the formation of DA-adducts.

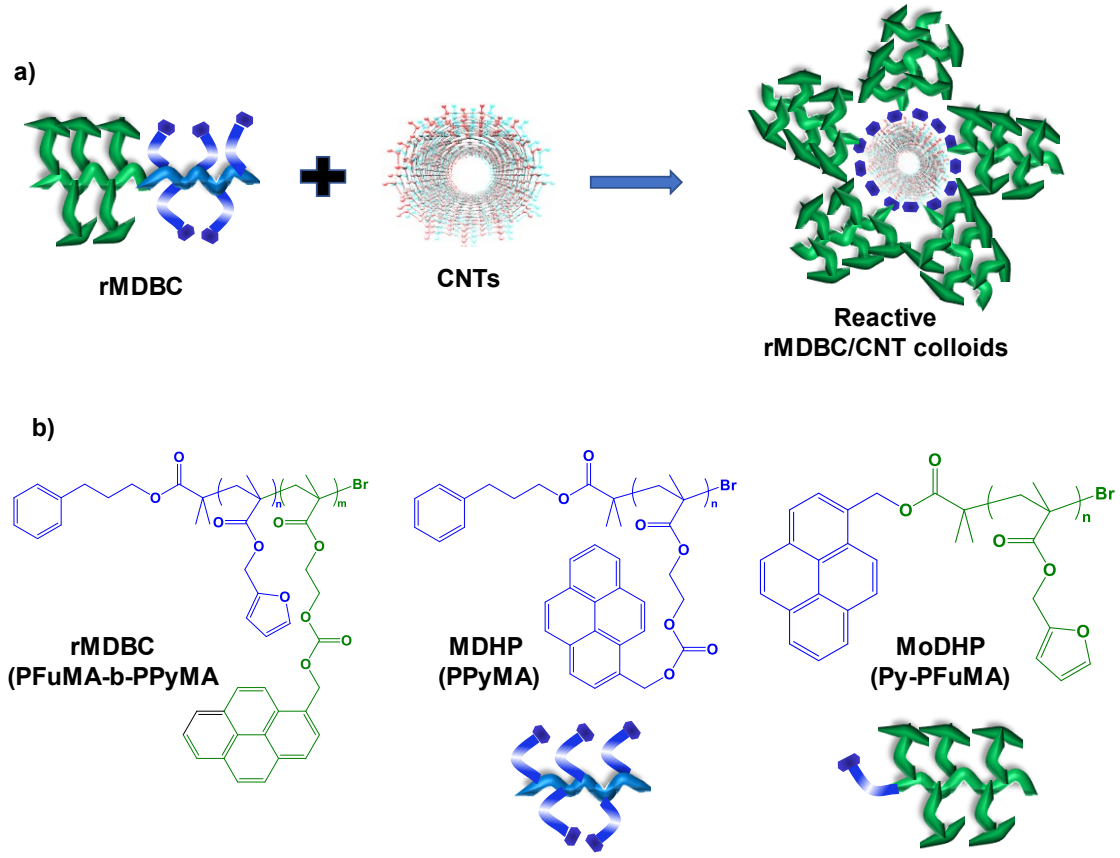


**Figure 2.1** Schematic illustration of stabilization of CNT surfaces with rMDBC to fabricate rMDBC/CNT colloids (a) and chemical structures of rMDBC, MDHP, and MoDHP (b).

## 2.2 Experimental section

### 2.2.1 Instrumentation

$^{1}$H- and $^{13}$C-NMR spectra were recorded using a 500 MHz Varian spectrometer with $CDCl_3$ singlet at 7.26 ppm as the reference standard. Monomer conversion was determined by $^{1}$H NMR analysis. Molecular weight analysis of (co)polymers were conducted by gel permeation chromatography (GPC). An Agilent GPC was equipped with a 1260 Infinity Isocratic Pump and a RI detector. Two Agilent PLgel mixed-C and mixed-D columns were used with DMF containing 0.1 mol% LiBr at 50 °C at a flow rate of 1.0 mL/min. Linear poly (methyl methacrylate) standards from Fluka were used for calibration. Aliquots of the polymer samples were dissolved in DMF/LiBr. The clear solutions were filtered using a 0.45 μm polytetrafluoroethylene (PTFE) filter to remove any DMF-insoluble species. A drop of anisole was added as a flow rate marker.

Thermogravimetric analysis (TGA) was carried out using a TA instrument Q50 analyzer. Typically, dried samples were placed in a platinum pan inside a programmable furnace. They were then heated from 25 to 800 ℃ at a heating rate of 10 ℃/min under nitrogen flow. Mass loss was then calculated. Differential scanning calorimetry (DSC) analysis including glass transition temperature ($T_g$) of copolymers were measured with a TA Instruments DSC Q20 differential scanning calorimeter. Samples were dried under vacuum for 24 hrs at room temperature to remove residual solvents. Temperature ranged from -80 to 200 ℃ for heating and cooking cycles conducted at a rate of 10 ℃/min. (Cycles: cool to from -80 ℃, heat up to 200 ℃ ($1^{st}$ run), cool to -80 ℃, heat up to 200 ℃ ($2^{nd}$ run), and cool to 25 ℃). The $T_g$ values were determined from the $2^{nd}$ heating run.

TEM images were obtained using a Philips Tecnai 12 TEM, operated at 80kV and equipped with a thermionic LaB6 filament. An AMT V601 DVC camera with point to point resolution and line resolution of 0.34 and 0.20 nm, respectively, was used to capture images at 2048 by 2048 pixels. To prepare specimens, aqueous dispersions were dropped onto copper TEM grids (400 mesh, carbon coated), blotted and allowed to air dry at room temperature.

### 2.2.2 Materials

1,1′-Carbonyldiimidazole (CDI, >97%), 1-pyrenemethanol (PyOH, 98%), triethylamine ($Et_3N$, 99.5%), bromoisobutyryl bromide (Br-iBuBr, 98%), 4-dimethylamino pyridine (DMAP, >99%), N,N,N′,N″,N″-pentamethyldiethylenetriamine (PMDETA, 99%), copper(I) bromide (Cu(I)Br, 99.999% trace metal basis), 1,1′-(methylenedi-4,1-phenylene) bismaleimide (BM, 95%) and multiwalled carbon nanotubes (CNTs, >98% carbon basis, O.D. × L 6-13 nm × 2.5-20 μm) were purchased from Sigma-Aldrich. Furfuryl methacrylate (FuMA, 97%) and 2-hydroxyethyl methacrylate (HEMA, >99%) from Aldrich were purified by passing through basic alumina column to remove inhibitors before polymerization. 3-Phenylpropyl 2-bromo-2-methylpropanoate (PP-Br) was synthesized as described in our publication.[33]

### 2.2.3 Synthesis of PyMA

In the first step to synthesize CI-MA, CDI (10.0 g, 61.7 mmol) dissolved in dichloromethane (DCM, 450 mL) was mixed with HEMA (6.2 mL, 51.4 mmol) dissolved in DCM (60 mL). After being stirred for 12 hrs at room temperature, the mixture was washed with water (200 mL) three times to remove excess CDI and by-products, and then dried over $Na_2SO_4$. After DCM was

removed by rotary evaporation, the product was dried in a vacuum oven at room temperature for 24 hrs, yielding 10.6 g (92%). TLC: $R_f$ = 0.3 (6/4 hexane/ethyl acetate); Mass for ($C_{10}H_{12}N_2O_4Na^+$) calculated: 247.06893 and found: 247.06916.

In the next step to synthesize PyMA, Py-OH (5.2 g, 22.3 mmol) dissolved in dichloromethane (5 mL) was mixed with a mixture of CIMA (5.0 g, 22.3 mmol) and $Et_3N$ (2.5 g, 24.5 mmol) in dichloromethane (70 mL) at room temperature. After 18 hrs, the solution was washed with aqueous brine solution (100 mL) twice. Solvent was removed by rotary evaporation and the product was purified by silica column chromatography with the mixture of hexane/ethyl acetate (7/3 v/v). The product was collected as the first of three bands of the silica column and dried in a vacuum oven at room temperature for 24 hrs, yielding 5.3 g (60.9 %). TLC: $R_f$ = 0.7 (6/4 hexane/ethyl acetate); Mass calculated for ($C_{24}H_{20}O_5Na^+$): 411.12029. Found: 411.11975.

### 2.2.4 Synthesis of Py-Br

A solution consisting of Py-OH (1.5 g, 6.5 mmol), $Et_3N$ (1.0 g, 10 mmol), DMAP (81.4mg, 666.3 umol) and iBuBr (1.7 g, 7.3 mmol) was dissolved in DCM (20 mL). After being stirred for 12 hrs at room temperature, DCM was removed by rotary evaporation. The formed product was dried in a vacuum oven at room temperature for 24 hrs, yielding 1.0 g (40 %). $R_f$ = 0.8 on silica (6/4 v/v HE/EA).

### 2.2.5 General procedure for ATRP

Initiator, monomer, PMDETA and anisole were added to a 20 mL Schlenk flask. The resulting mixture was deoxygenated by three freeze-pump-thaw cycles. The reaction flask was filled with nitrogen and Cu(I)Br was added to the frozen solution. The flask was sealed, purged with vacuum, and backfilled with nitrogen. After the mixture was thawed, the flask was immersed in an oil-bath preheated to the desired temperature (40 °C) to start the polymerization. Aliquots were withdrawn at given time intervals to characterize the conversion of monomers and the molecular weight of the formed copolymers.

For purification, the as-synthesized polymer solutions were precipitated from hexane to remove unreacted monomers. The precipitates were dissolved in THF and passed through basic alumina column to remove residual copper species. Solvents were removed by rotary evaporation and the residues were dried in a vacuum oven at room temperature for 24 hrs.

***Synthesis***: PP-Br (0.2 g, 0.77 mmol), FuMA (4.5 g, 38.7 mmol), PMDETA (56.4 mg, 325.4 μmol), Cu(I)Br (22.2 mg, 154.9 μmol), and anisole (11.3 mL) for PFuMA-Br; PFuMA-Br (0.22 g, 64.8 μmol), PyMA (1.3 g, 3.24 mmol), PMDETA (4.7 mg, 27.2 μmol), Cu(I)Br (2.8 mg, 19.4 μmol) and anisole (5.3 mL) for PFuMA-b-PPyMA (rMDBC); PP-Br (30.0 mg, 0.12 mmol), PyMA (2.3 g, 5.8 mmol), PMDETA (8.5 mg, 48.8 μmol), Cu(I)Br (3.3 mg, 23.2 μmol) and anisole (5.7 mL) for PPyMA (MDHP); and Py-Br (173.3 mg, 452.1 μmol), FuMA (2.6 g, 22.6 mmol), PMDETA (32.9 mg, 189.9 μmol), Cu(I)Br (13.0 mg, 90.4 μmol) and anisole (6.6 mL) for Py-PFuMA (MoDHP).

### 2.2.6 Determination of correlation factors using UV/vis spectroscopy

A series of polymer solutions in anisole at various concentrations of 5, 10, 15, and 20 μg/mL for rMDBC and 80, 200, 300, 400 and 500 μg/mL for MoDHP were prepared. Their UV/vis spectra were recorded and the absorbance at 347 nm was plotted over the mount of polymers in anisole as mg/mL.

### 2.2.7 Investigation of binding affinity

A given amount of CNTs (10 mg) was mixed with various amounts of rMDBC (5, 10, 30, 40, 50, 70, 100 mg) in anisole (5 mL). The resulting mixtures were stirred at room temperature for 24 hrs and then were subjected to centrifugation (8000 rpm x 20 min x 25 °C). Supernatants were carefully decanted and further filtered with a PTFE disc-type filter (diameter 0.45 μm). The resultant clear solutions after being diluted were recorded with UV/vis spectroscopy.

For comparison with rMDBC, the similar procedure except for filtration with PTFE filter was applied for the dried MDHP and MoDHP (10 mg) mixed with CNTs (10 mg) at 1/1 wt/wt CNT/polymer in anisole (5 mL). Further, the precipitates of MDHP/CNT hybrids were analyzed by TGA to determine the amount of MDHP in the precipitate.

### 2.2.8 Gel-sol-gel experiments

A dispersion of 7/1 wt/wt rMDBC/CNT colloids in anisole (0.2 mL, 14 mg/mL) was mixed with BM (4.3 mg, 12 μmol) and additional rMDBC (128.4 mg, 12 μmol) in anisole (0.2 mL) in a 10 mL vial. The formed reactive mixture was kept at 50 °C for 2 hrs, forming standing gel, heated at 120 °C for 2 hrs, forming a sol, and cooled to and kept at 50 °C, reforming standing

gel. The gel was dried in a vacuum oven set at 50 °C for 2 days and characterize its thermal analysis.

## 2.3 Results and Discussion

### 2.3.1 Synthesis of PyMA

As depicted in Figure 2.2, our route with two steps to synthesize a novel PyMA begins with the synthesis of a CIMA precursor by the reaction of HEMA with CDI, which was straightforward with no need of any catalysts. The product was purified by washing with water three times at a yield of as high as 92 %. $^{1}$H-NMR spectrum in Figure S2.1a shows the presence of imidazole moieties (e, f, g) and methacrylate moieties (a). Next step is the reaction of the purified CIMA with Py-OH in the presence of $Et_3N$ as a base catalyst. The product was purified by column chromatography at a yield of 58%. $^{1}$H-NMR spectrum in Figure S2.1b shows the disappearance of the peaks at 7.0-8.5 ppm corresponding to imidazole moieties and the appearance of the new peaks at 8.0-8.5 ppm equivalent to pyrene moieties. The $^{1}$H-NMR analysis, combined with $^{13}$C-NMR analysis for CIMA (Figure S2.2) and PyMA (Figure S2.3) as well as their mass spectroscopic analysis, confirm the successful synthesis of CIMA and PyMA.

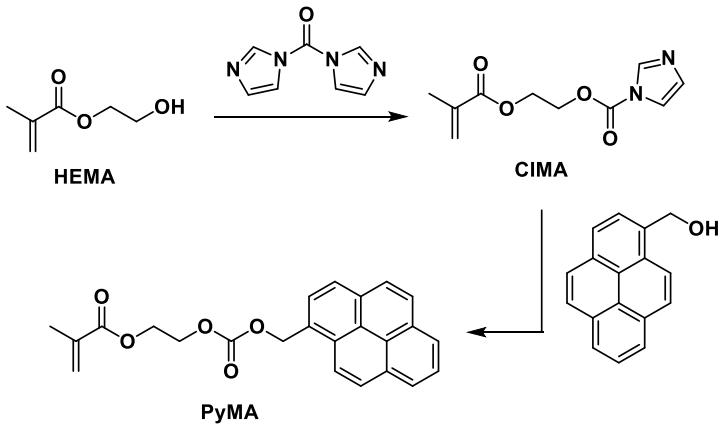


**Figure 2.2** Synthesis of PyMA.

### 2.3.2 Synthesis of rMDBC and kinetic investigation

Figure 2.3 illustrates our approach to synthesize well-controlled rMDBCs with pre-determined molecular weight and narrow molecular weight distribution. With a choice of PP-Br as an ATRP initiator, consecutive atom transfer radical polymerization (ATRP)[127, 128] was

examined with FuMA in the first step to synthesize PFuMA-Br macroinitiator and PyMA in the second step for chain extension of PFuMA with PPyMA, yielding well-defined PFuMA-b-PPyMA block copolymers.

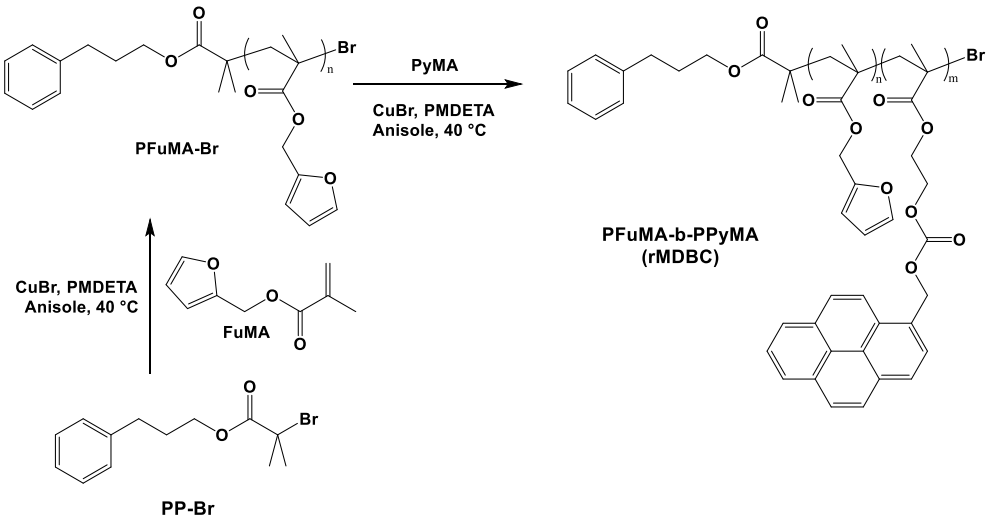


**Figure 2.3** Synthesis of well-controlled rMDBC by consecutive ATRP.

ATRP technique has been explored to synthesize well-controlled PFuMA in literature.[32, 129] In our experiment to synthesize PFuMA-Br macroinitiator as the first step, ATRP of FuMA was initiated with PP-Br in the presence of Cu(I)Br/PMDETA active catalysts in anisole at 40 °C. The initial mole ratio of $[FuMA]_0/[PP\text{-}Br]_0$ was set to be 50/1 as projecting the degree of polymerization (DP) to be 50 at complete monomer conversion. At 48 % monomer conversion, the formed polymer was purified by standard method including precipitation from a poor solvent (here, hexane) to remove residual FuMA monomers and passing through basic aluminum oxide to remove residual metal species. $^1$H-NMR in Figure 2.4a shows the presence of furfuryl groups (f) and initiating species (c). Using their integrals, the DP of PFuMA was determined to be 27. GPC analysis confirms that the PFuMA-Br had the number average molecular weight ($M_n$) = 8.6 kg/mol with narrow dispersity as Đ <1.33 (Figure S2.4).

In the second step, the purified PFuMA-Br was used as a macroinitiator for ATRP of PyMA in the presence of CuBr/PMDETA active catalysts in anisole at 40 °C, with a choice of the $[PyMA]_o/[PFuMA\text{-}Br]_o$ = 50/1. After being purified by standard method, the formed product was analyzed. $^1$H-NMR in Figure 2.4b shows the presence of furfuryl groups in the PFuMA block (f)

and pyrene groups (p) in the PPYMA block. Their integral ratio, along with the DP of PFuMA = 27, allows to determine the DP of PPyMA block to be 23. GPC diagram of the product was clearly shifted to high molecular weight region with no significant trace of PFuMA-Br macroinitiator as well as with an increase of $M_n$ to 19.5 kg/mol and narrow dispersity as Đ <1.24 (Figure S2.4). These results suggest that our approach utilizing consecutive ATRP technique enabled the synthesis of well-controlled $PFuMA_{27}$-b-$PPyMA_{23}$ block copolymer.

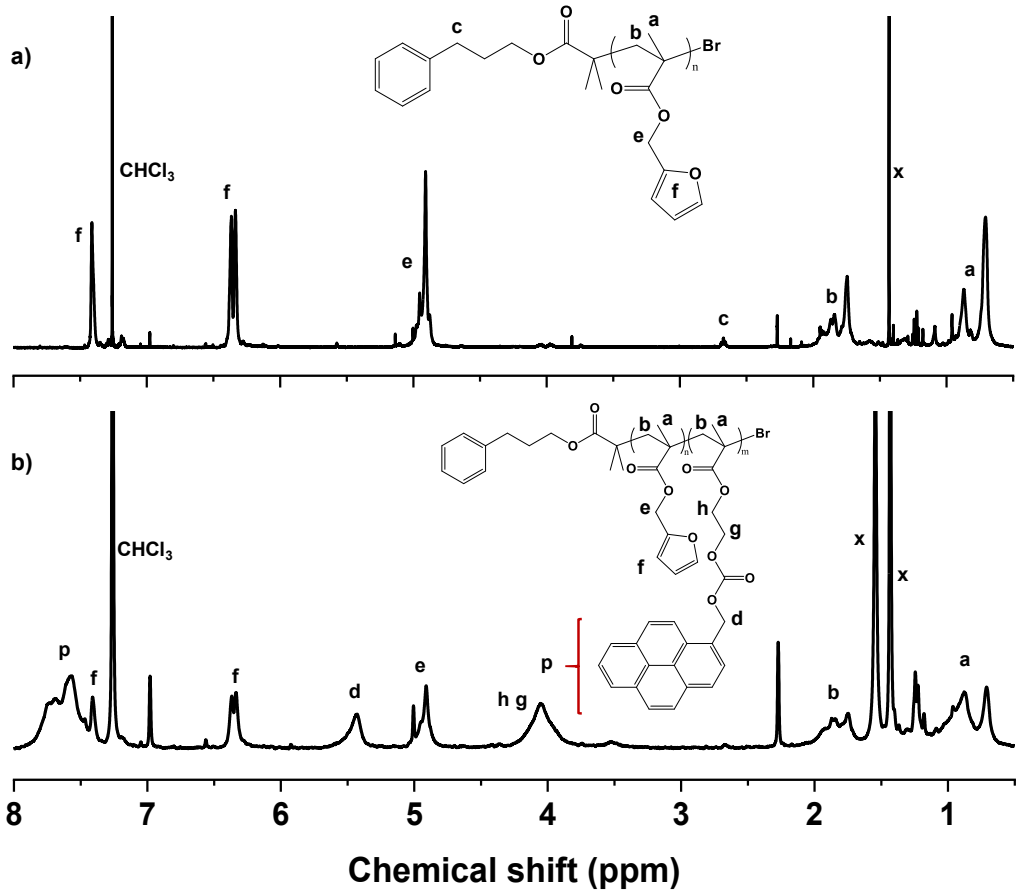


**Figure 2.4** $^1$H-NMR spectra of PFuMA-Br macroinitiator (a) and PFuMA-b-PPyMA block copolymer (b) in $CDCl_3$. Conditions for ATRP: $[FuMA]_o/[PP\text{-}Br]_o/[Cu(I)Br]_o/[PMDETA]_o$ = 50/1/0.2/0.3 in anisole at 35 °C with FuMA/anisole = 0.4/1 wt/wt for PFuMA-Br; $[PyMA]_o/[PFuMA\text{-}Br]_o/[Cu(I)Br\text{-}PMDETA]_o$ = 50/1/0.7 in anisole at 40 °C with PyMA/anisole = 0.24/1 wt/wt for PFuMA-b-PPyMA.

In another set of our experiments, the kinetics of ATRP block copolymerization was investigated with different initial mole ratios of $[PyMA]_0/[PFuMA\text{-}Br]_0$ = 50/1 and 100/1. As seen in Figure S2.5, all polymerizations were well-controlled, with first order kinetics, linear increase in molecular weight over conversion, and narrow molecular weight distribution (Đ <1.3) as well as evolution of GPC diagrams to high molecular region over conversion. As expected, polymerization was faster with $[PyMA]_0/[PFuMA\text{-}Br]_0$ = 50/1 than 100/1 under the similar conditions including the same PyMA/anisole = 0.2/1 wt/wt.

### 2.3.3 Synthesis of control MDHP and MoDHP for comparison

Our synthetic approach to synthesize a well-defined PPyMA homopolymer (MDHP) utilizes the ATRP of PyMA initiated with PP-Br at the $[PyMA]_0/[PP\text{-}Br]_0$ = 50/1 in anisole at 40 °C (Figure S2.6a). $^1$H-NMR spectrum in Figure S2.6b shows the pyrene moieties (p) in PPyMA and the methylene groups in initiating species (c). Using their integral ratio, the DP of PPyMA was determined to be 14. The formed copolymer had the $M_n$ = 8.0 kg/mol and Đ = 1.32 by GPC (Figure S2.7). Figure S2.8a illustrates our approach to synthesize monodentate Py-PFuMA homopolymer (MoDHP). First, a novel Py-Br initiator was synthesized by a facile coupling reaction of Py-OH with Br-iBuBr. $^1$H-NMR spectrum in Figure S2.8b shows the characteristic peaks at 8.0-8.5 ppm presenting pyrene moieties (p) and 1.9 ppm corresponding to two methyl groups (b). Their integral ratio confirms >97% conjugation efficiency. Next, the purified Py-Br was used as an initiator for ATRP of FuMA to synthesize Py-PFuMA. $^1$H-NMR spectrum presents pyrene moieties and pendant furfuryl groups. Using their integral ratio, the DP of PFuMA was determined to be 24. The formed Py-PFuMA had the $M_n$ = 8.3 kg/mol with Đ = 1.38 by GPC (Figure S2.9).

### 2.3.4 Thermal analysis

The formed block copolymer and homopolymers for comparison were characterized for their thermal properties using DSC (Figure S2.10) and TGA (Figure S2.11). DSC analysis shows that rMDBC block copolymer consisting of PFuMA and PPyMA blocks had one glass transition temperature ($T_g$) at 69 °C, suggesting that PFuMA and PPyMA blocks are miscible. Note that the $T_g$ was determined to be 51 °C for PFuMA-Br precursor and 53 °C for PPyMA-Br (i.e. MDHC) homopolymers. Interestingly, MoDHP had its $T_g$ of 56 °C, which is close to that of PFuMA-Br, suggesting no significant effect of terminal pyryl and phenyl groups on the thermal properties of

PFuMA homopolymers. TGA analysis show the progressive decompositions of the (co)polymers to around 450 °C. All the (co)polymers had 10-20% residues, which is presumably due to aromatic rings (pyrene and furan groups) in the (co)polymers.

### 2.3.5 Binding affinity of rMDBC on CNTs and comparison with control homopolymers

Pyrene groups can anchor to the surfaces of CNTs through non-covalent π-π interactions. Thus, the binding ability of rMDBC consisting of a pendant pyrene block on CNT surfaces was investigated to prepare CNTs stabilized with rMDBCs (rMDBC/CNT colloids). A given amount of CNT was mixed with various amounts of rMDBC under stirring to prepare a series of rMDBC/CNT colloids with different weight ratios from 0.5/1 to 10/1 in anisole. Figure 2.5 shows the schematic illustration of our protocol to quantitatively investigate the stabilization of CNTs with reactive rMDBC at 1/1 wt/wt CNT/rMDBC ratio. Figure 2.5a and 2.5b demonstrate the improved colloidal stability of CNTs mixed with rMDBC, compared with CNTs without rMDBC. CNTs without rMDBC were rapidly precipitated in anisole. Promisingly CNTs with rMDBC were stably dispersed in anisole over a week. Such enhanced colloidal stability could be attributed to the stabilization of CNT surfaces with multiple pyrene groups as multidentate ligands, yielding colloidally stable rMDBC/CNT hybrids. Note that their precipitation gradually proceeded over time on shelf.

The resultant rMDBC/CNT hybrids were characterized for morphologies by TEM. As seen in Figure 2.5d and 2.5e, TEM images with low and high magnifications of bare CNTs show prototype CNTs as long bundles with the average diameter of ca 10 nm. In contrast, rMDBC/CNT hybrids appeared to be shorter in their lengths, which could be due to mechanical shear generated by magnetic stirring during stabilization process (Figure 2.5f and 2.5g). Their diameters appeared to be increased, with the average diameter to be ca. 20 nm, which could suggest the presence of rMDBCs on CNT surfaces.

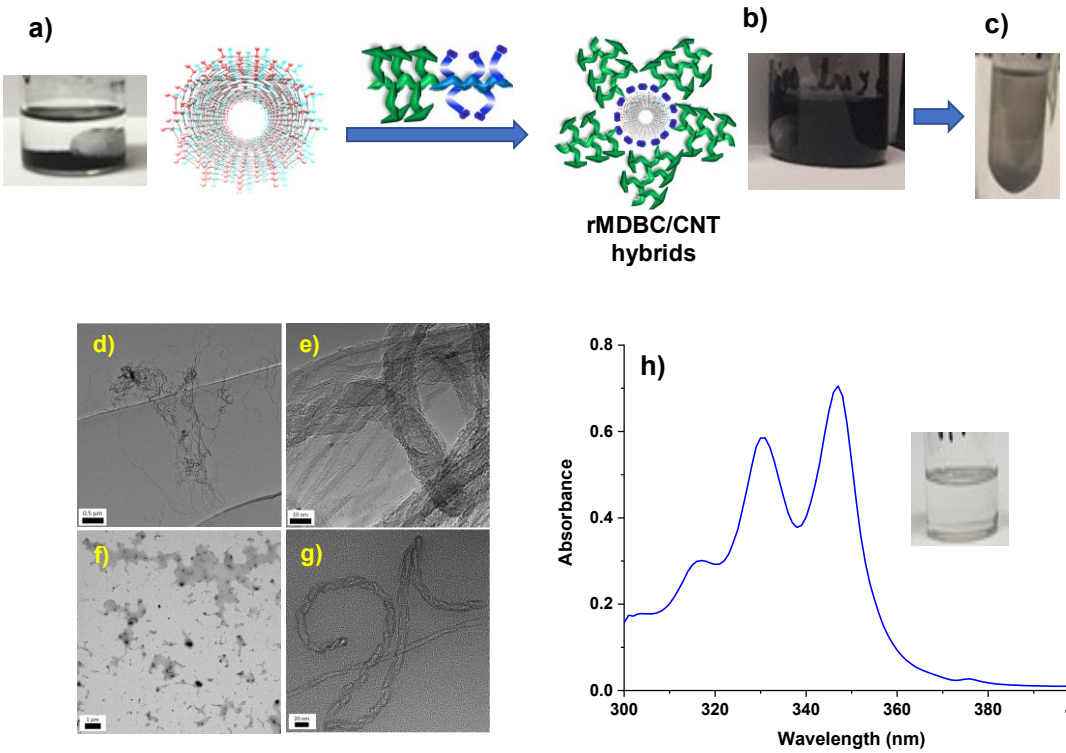


**Figure 2.5** Schematic illustration and digital images of CNTs without (a) and with (b) rMDBC in anisole at 1/1 wt/wt rMDBC/CNT ratio; digital image of the resultant dispersion after centrifugation (c); TEM images with different magnifications for 1/1 wt/wt rMDBC/CNT hybrids (f, g), compared with those for bare CNTs (d, e). Scale bar = 1 µm (d), 20 nm (e), 0.5 µm (f), and 10 nm (g); and UV/vis spectrum upon dilution of supernatant after filtration with PFFE filter and digital image in inset (h).

Next, the affinity of rMDBC on CNT surfaces was quantitatively analyzed using UV/vis spectroscopy to determine the amount of free (unbound to CNTs) rMDBC in the separated supernatant after centrifugation. As seen in Figure 2.5c, however, the centrifugation to separation was not straightforward. The supernatant was not clear, but slightly dark with residual CNTs. To proceed our analysis, the supernatant solutions were subjected to filtration with PTFE filters (Figure 2.5h, inset). The resultant solutions were clear and thus recorded using UV/vis spectroscopy (Figure 2.5h). The correlation curve was built with the absorbance of pyrene species at 347 nm over the amount of rMDBC. As seen in Figure S2.12, the slop was determined to be 41.7 $(mg/mL)^{-1}$.

With this correlation curve and the absorbance of rMDBC in supernatant at 347 nm, the amount of rMDBC in rMDBC/CNT hybrids as well as the efficiency of rMDBC to bind to CNT

surfaces were determined. Figure 2.6a shows the results. At the 0.5/1 of rMDBC/CNT ratio (equivalent to 33% rMDBC), the amount of rMDBC in the hybrid was around 32%, which correspond to >95% binding efficiency. With an increasing amount of rMDBC in the mixtures as an increasing wt ratio of rMDBC/SNP to 4/1, the amount of rMDBC increased to 55%. Upon the further increase, the amount of rMDBC in the hybrids decreased to reach to plateau at 35%. The plausible reason for such decrease could be attributed to the saturation of solution with excess rMDBC. As expected, the binding efficiency continued to decrease to <10% when the amount of rMDBC increased in the mixtures.

Further, the binding efficiency on CNT surfaces was determined for MDHC (a multidentate homopolymer) and MoDHP (a monodentate) for comparison with rMDBC. With the choice of rMDBC/CNT = 1/1 wt/wt, the similar protocol with UV/vis spectroscopy was used. The results are compared in Figure 2.6b. Different from rMDBC/CNT mixtures, both MDHC/CNT and MoDHP/CNT mixtures show clear separation and thus no additional filtration was required to separate free polymers. For MDHP with pendant multiple pyrene groups, the amount of MDHP in MDHP/CNT hybrids were determined to be 26.3 % using UV/vis spectroscopy with the slope (41.2 $(mg/mL)^{-1}$) determined for rMDBC. To validate, TGA analysis was conducted for the precipitate of MDHP/CNT hybrids. As analyzed in Figure S2.13, the binding efficiency was estimated to be 32%, which is close to that (26.3%) determined using UV/Vis spectroscopy. For MoDHP, its correlation factor was determined to be 7.1 $(mg/mL)^{-1}$ using UV/vis spectroscopy (see Figure S2.14) and used to determine the amount of MoDHP in MoDHP/CNT hybrids to be 26%. Overall, rMDBC had greater binding efficiency (60%) over both MDHP and MoDHP, suggesting the clear advantages for the use of MDBC over homopolymers and monodentates for the stabilization of CNT surfaces.

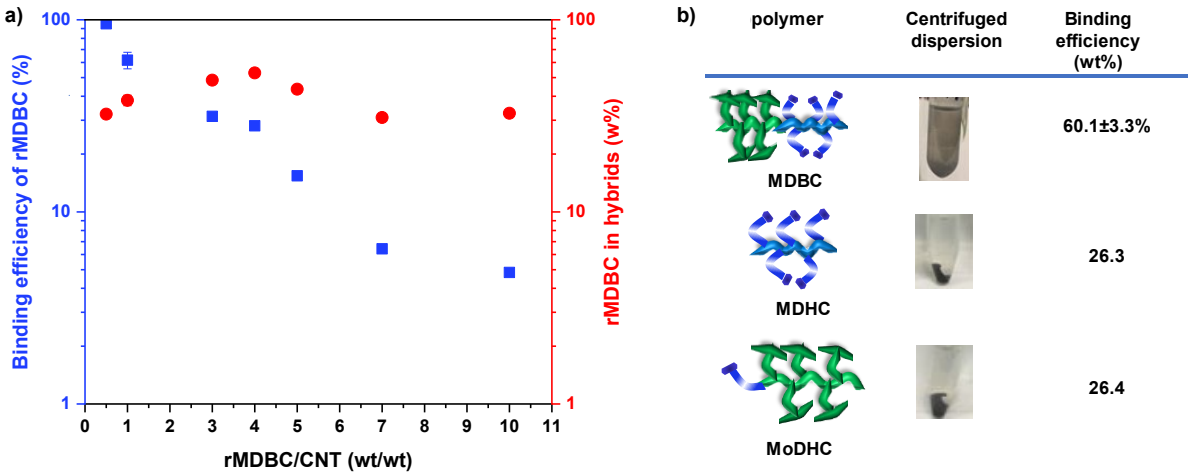


**Figure 2.6** Binding ability of rMDBC to CNT surfaces for a series of mixtures at various rMDBC/CNT weight ratio (a) and schematic illustration to important advantages for the use rMDBC over MDHC and MoDHC for the stabilization of CNT surfaces. Conditions for experiments: polymer/CNT = 1/1 wt/wt (b).

### 2.3.6 Gel-sol-gel transition through dynamic DA/rDA chemistry

As schematically illustrated in Figure 2.7a, the resultant rMDBC/CNT hybrids are composed of pendant furfuryl groups that can be reactive to polymaleimides to yield dynamic gel networks through the formation of DA cyclic adduct linkages. At elevated temperature, the resultant DA-crosslinked networks can be dissociated to the corresponding precursors (i.e. rMDBC/CNT hybrids and polymaleimides) upon the cleavage of the DA linkages. When being cooled, the dissociated products can be subjected to DA reactions to reform dynamic crosslinked networks. Figure 2.7b-2.7e shows sol-gel transition resulted from dynamic DA/rDA chemistry. When a reactive mixture consisting of rMDBC/CNT hybrids and BM (a dimaleimide) shown in Figure 2.7b was kept at 50 °C, it turned to be a standing gel in a vial through DA reaction (Figure 2.7c). Being heated at 120 °C, the gel became a sol through rDA reaction where the DA crosslinks are cleaved to the corresponding maleimides and furan species. (Figure 2.7d). The resultant sol turned to standing gel upon maintaining temperature at 50 °C (Figure 2.7e). After being dried, the gel was characterized for its thermal property using TGA (Figure S2.15). Analysis of weight loss at 700 °C confirms the amount of CNT to be 0.5%, which is very close to that (0.3%) calculated from the recipe. We currently investigate the use of versatile rMDBC/CNT hybrids as

multivalent crosslinkers for the development of self-healable polyurethane networks through DA/rDA chemistry.

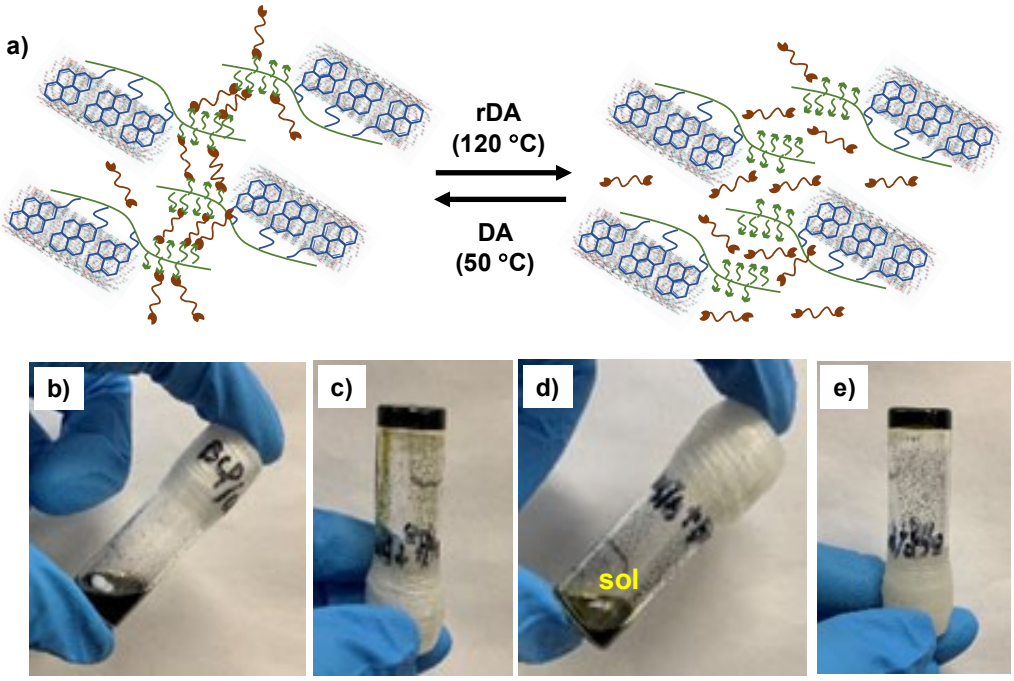


**Figure 2.7** Schematic illustration (a) and (b-e) digital images to show gel-sol-gel transition through thermoreversibility of a reactive mixture consisting of MDBC/CNT colloids and BM in anisole at room temperature (b), being kept at 50 °C for 2 hrs to form standing gel (c), heated at 120 °C for 2 hrs to sol (d), and cooled to and kept at 50 °C to reform standing gel (e). Condition for experiment: 25 wt% of solids consisting of rMDBC, CNT, and BM in anisole; 0.3 wt% CNTs based on rMDBC/CNT colloids; 1/1 mole equivalent ratio of furfuryl (in rMDBC) to maleimide (in BM) groups.

## 2.4 Conclusion

A new rMDBC stabilization strategy was investigated with the synthesis of a well-controlled PFuMA-b-PPyMA as an effective rMDBC having pendant furfuryl groups in one block and pyrene groups in the reactive block by consecutive ATRP technique. The polymerizations were well-controlled with first-order kinetics, linear increase of molecular weight, and narrow molecular weight distribution over conversion. The synthesized rMDBC turned to be effective to stabilize CNT surfaces; thus its binding ability to CNTs was greater compared with the counterparts of a homopolymer bearing pendant pyrene groups and a monodentate homopolymer labeled with a terminal pyrene group, confirmed by spectroscopic and TEM analysis. Our

preliminary results obtained from gel-sol-gel transition and thermal analysis suggest that the formed rMDBC/CNT colloids can be integrated as multiple crosslinkers to thermoreversible DA-crosslinked networks where CNTs are covalently embedded, thus exhibiting thermoreversible self-healing through dynamic DA/rDA chemistry.

## 2.5 Supporting Information

**Figure S2.1** $^{1}$H-NMR spectra of CIMA (a) and PyMA (b) in $CDCl_3$.

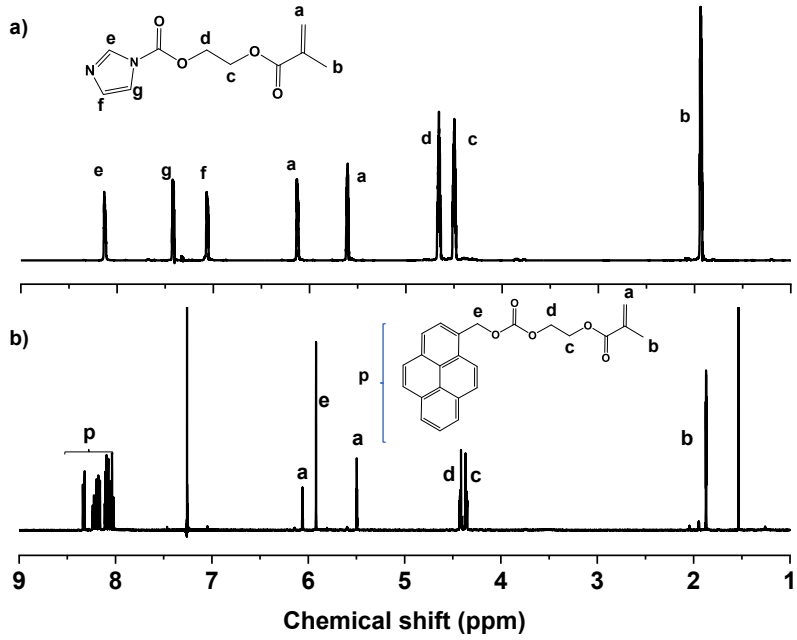


**Figure S2.2** $^{13}$C-NMR spectrum of CDIMA precursor in $CDCl_3$.

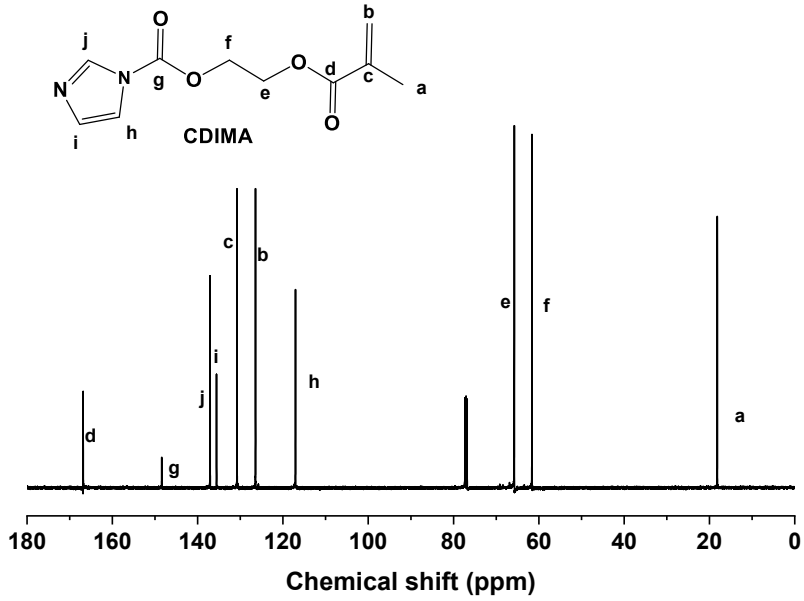

**Figure S2.3** $^{13}$C-NMR spectrum of PyMA in $CDCl_3$.

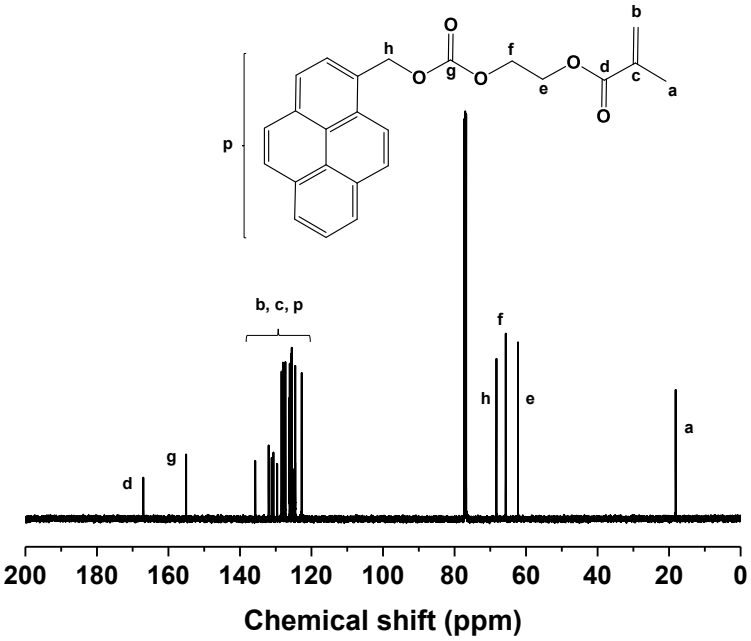


**Figure S2.4** Molecular weight distributions of PFuMA-Br precursor and PFuMA-b-PPyMA block copolymer.

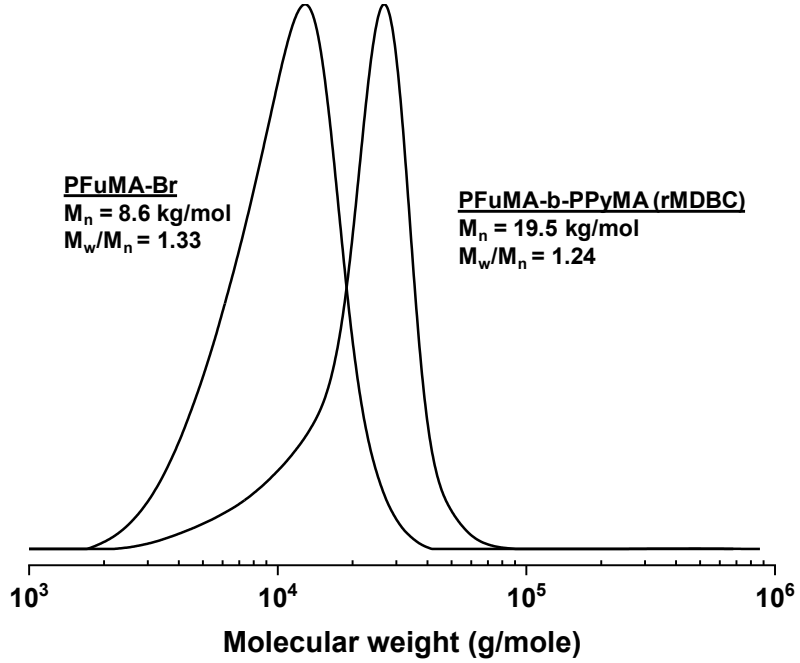

**Figure S2.5** First order kinetic plot over polymerization time (a), molecular weight and molecular weight distribution over conversion (b), and evolution of molecular weight distributions over conversion for ATRP of PyMA in the presence of PFuMA-Br macroinitiator with the initial mole ratio of $[PyMA]_o/[PFuMA\text{-}Br]_o$ = 50/1 (c) and 100/1 (d). The straight lines in (b) are theoretically calculated $M_n$ values at conversion. Conditions: $[PyMA]_o/[PFuMA\text{-}Br]_o/[Cu(I)Br\text{-}PMDETA]_o$ = 50/1/0.7 and 100/1/0.95 in anisole at 40 °C; PyMA/anisole = 0.24 wt/wt.

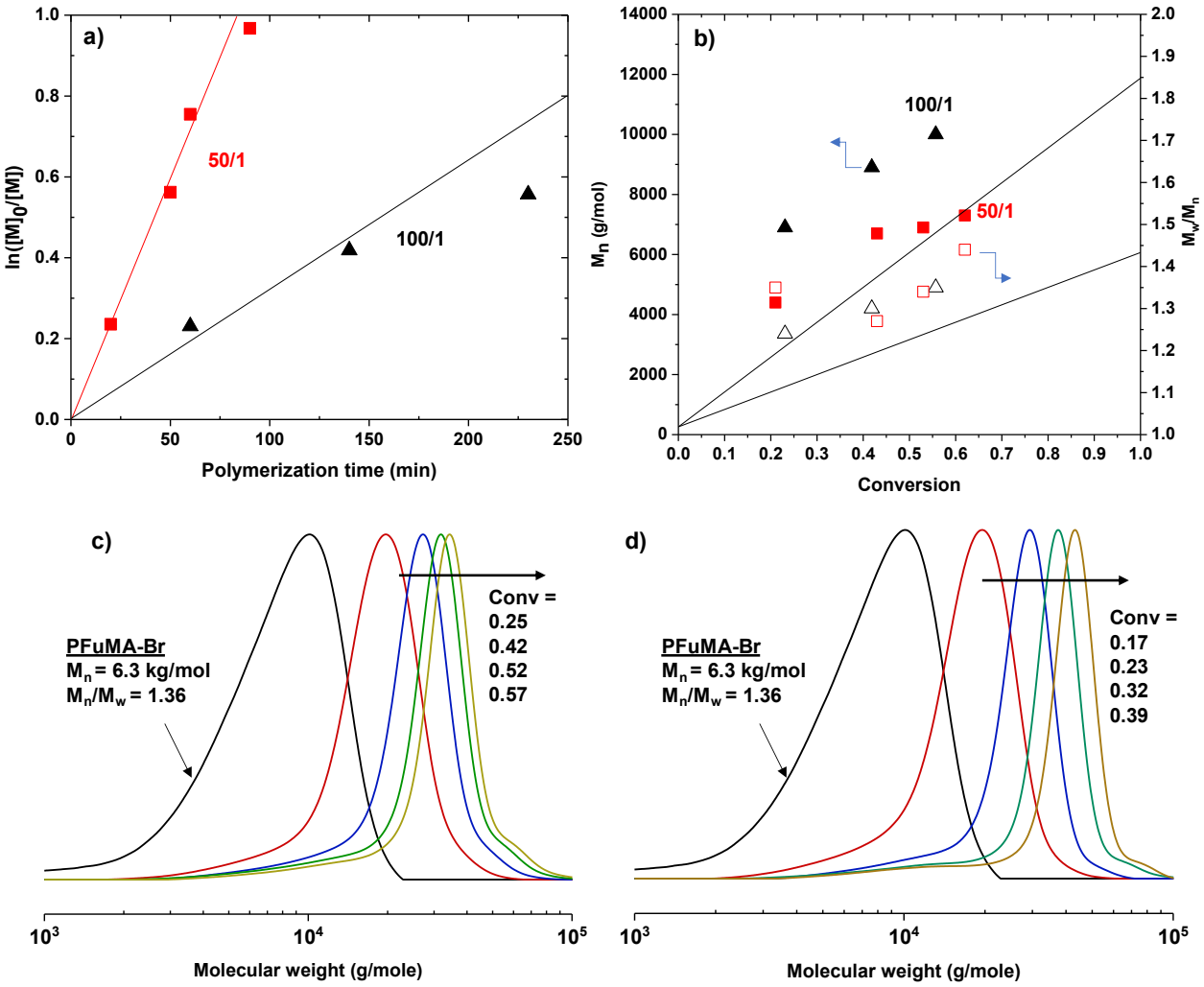

**Figure S2.6** Synthesis (a) and $^{1}$H-NMR spectrum in $CDCl_3$ (b) of PPyMA homopolymer. Conditions for ATRP: $[PyMA]_o/[PP\text{-}Br]_o/[Cu(I)Br\text{-}PMDETA]_o = 50/1/0.4$; PyMA/anisole = 0.4/1 wt/wt in anisole at 40 °C. Note that x in $^{1}$H-NMR spectrum denotes impurities, residual solvents, or water.

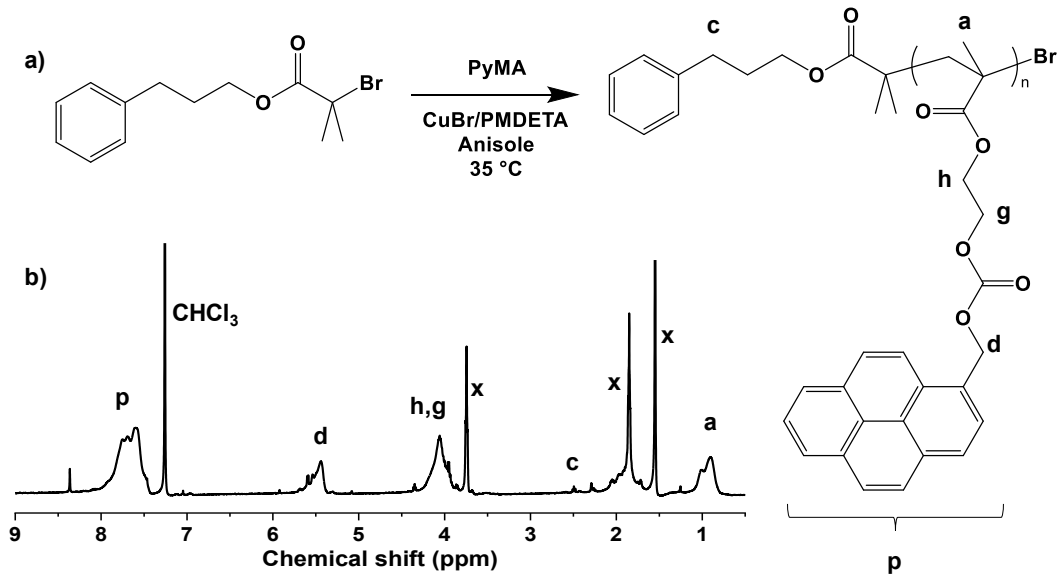


**Figure S2.7** Molecular weight distribution of PPyMA homopolymer.

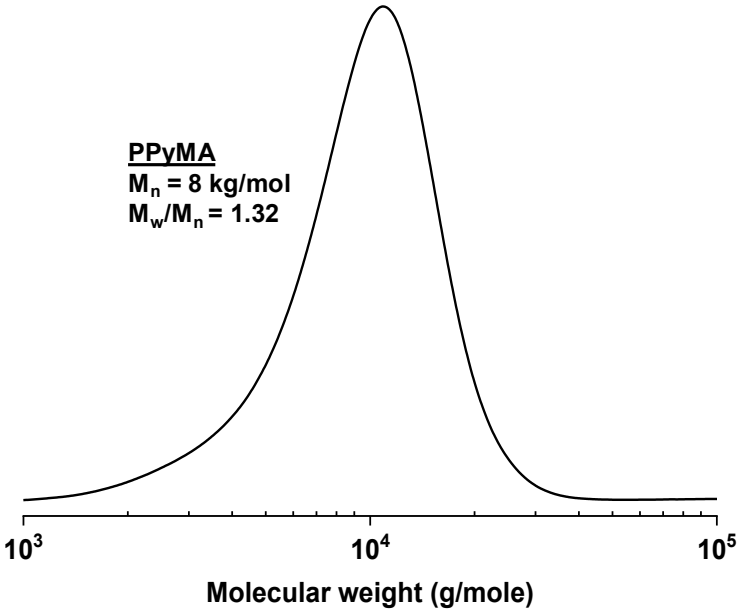

**Figure S2.8** Synthesis (a) and $^{1}$H-NMR spectra in $CDCl_3$ (b) of Py-Br and well-controlled Py-PFuMA homopolymer. Conditions for ATRP: $[FuMA]_o/[Py\text{-}Br]_o/[Cu(I)Br\text{-}PMDETA]_o$ = 50/1/0.4; FuMA/anisole = 0.4/1 wt/wt in anisole at 40 °C. Note that 1.57 in $^{1}$H-NMR spectrum denotes impurities, residual solvents, or water.

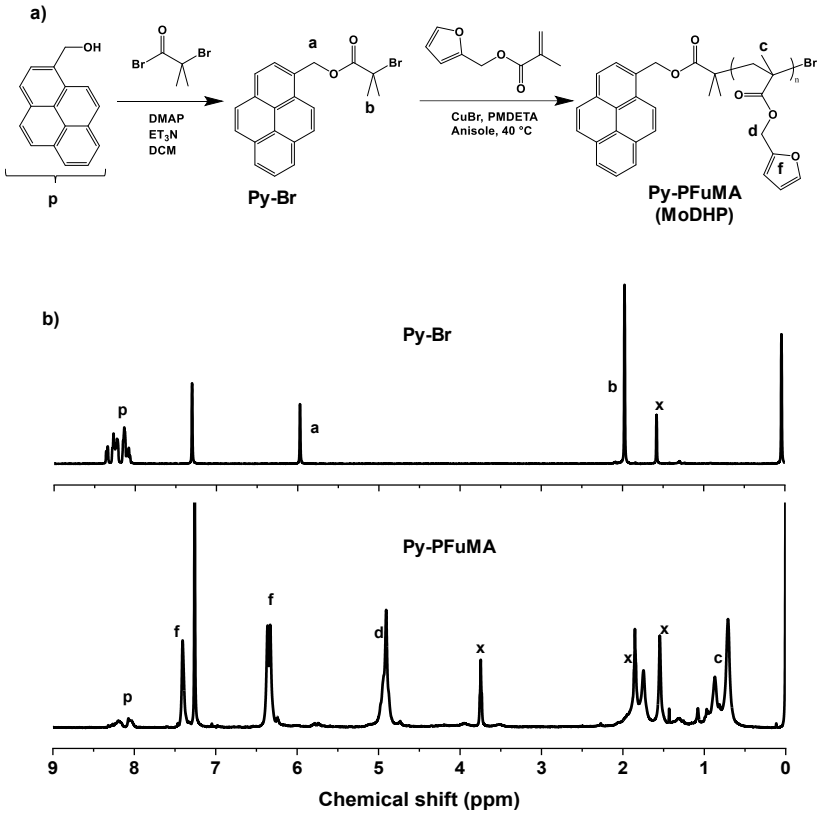


**Figure S2.9** Molecular weight distribution of monodentate Py-PFuMA homopolymer.

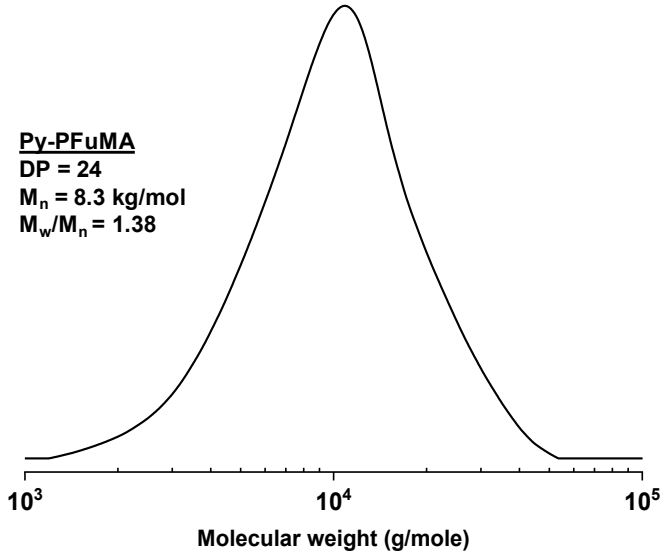

**Figure S2.10** DSC histogram (2nd heating run) of PFuMA-b-PPyMA block copolymer, compared with those of PFuMA, PPyMA homopolymers as well as Py-PFuMA. Cycles for DSC measurement: cool to from -80 ℃, heat up to 200 ℃ (1st run), cool to -80 ℃, heat up to 200 ℃ (2nd run), and cool to 25 ℃.

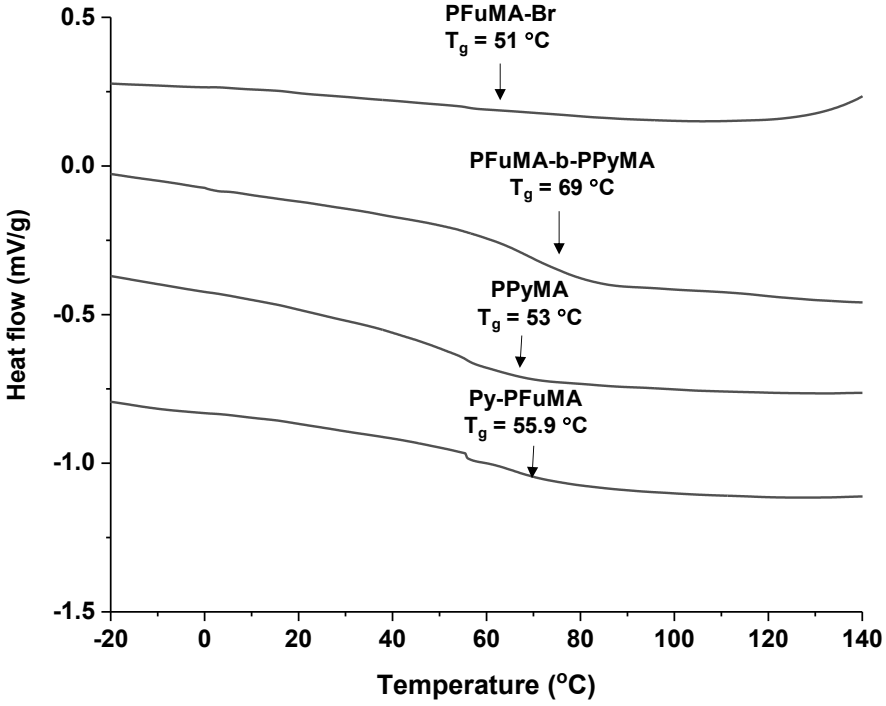


**Figure S2.11** TGA curves of PFuMA-b-PPyMA, compared with PFuMA-Br, PPyMA homopolymers as well as monodentate Py-PFuMA.

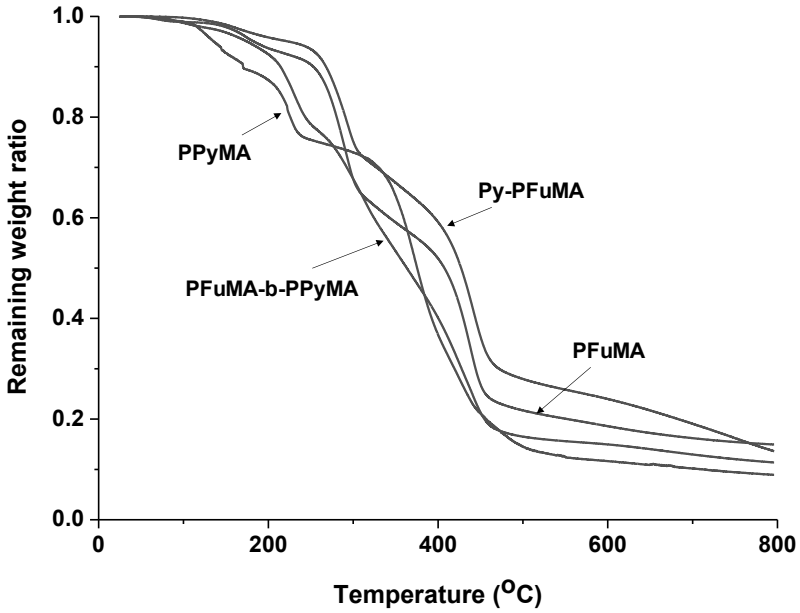

**Figure S2.12** Correlation plot of absorbance vs rMDBC amount in anisole. Inset: overlaid UV/vis spectra of rMDBC at various amounts in anisole.

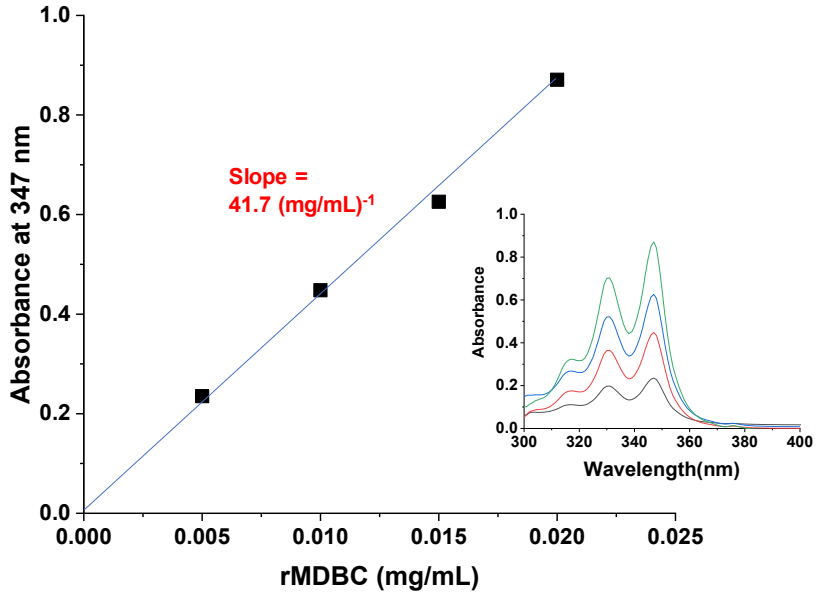


**Figure S2.13** TGA curves of PPyMA/CNT hybrids, compared with PPyMA and CNTs.

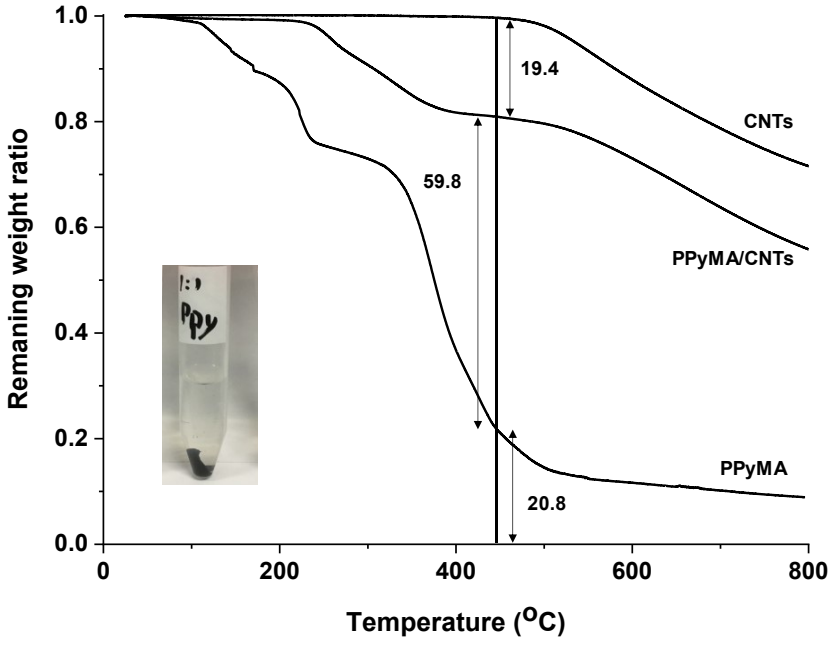


**Figure S2.14** Overlaid UV/vis spectra of MoDHP at various amounts in anisole (a) correlation plot of absorbance vs amount of MoDHP at 347 nm (b).

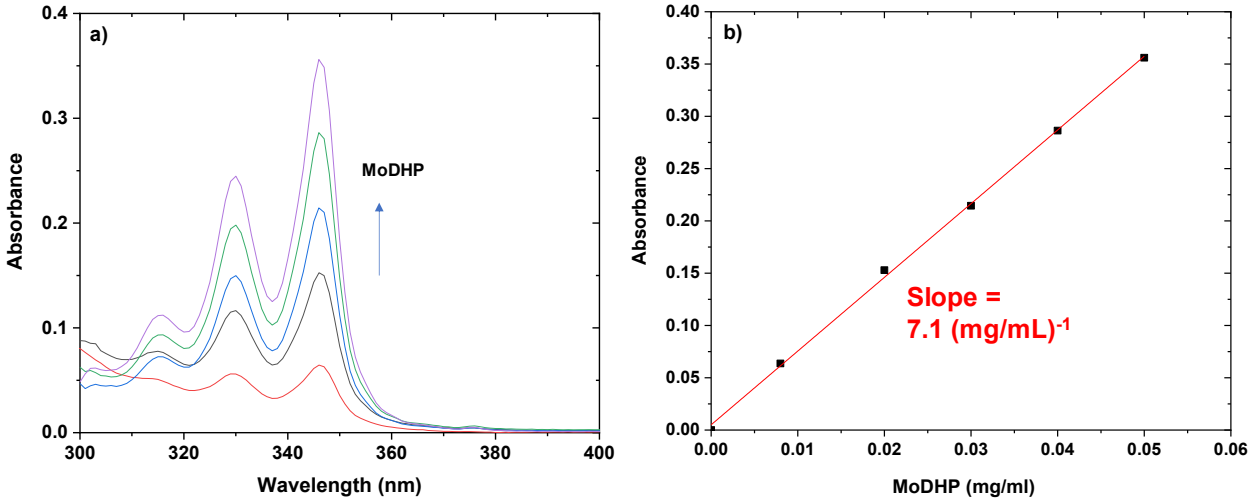


**Figure S2.15** TGA traces of dried gels prepared from a reactive mixture consisting of rMDBC/CNT hybrids and BM in anisole, compared with their precursors.

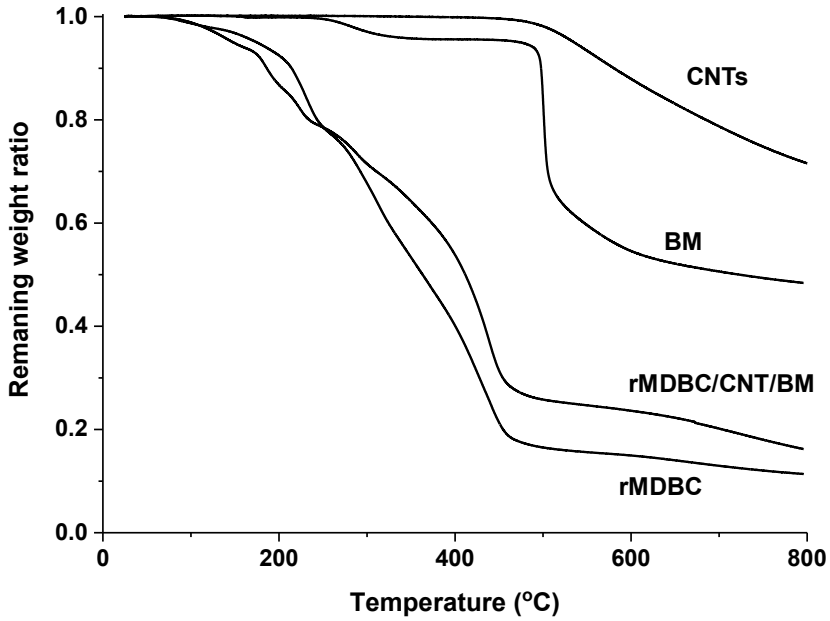

# Chapter 3
# Macromolecularly-engineered thermoreversible polyurethane hybrid networks encapsulating reactive multidentate block copolymer-stabilized carbon nanotubes

## 3.1 Introduction

Most intrinsic self-healing materials, based on reversible linkages, have been developed with soft polymers to foster void-filling ability in cracks and damaged area.[26, 48] The current and future design of robust self-healable networks requires a balance between toughness and flexibility. An appealing strategy towards a successful application involves the incorporation of nano particles, particularly carbon nanotubes (CNTs), into soft self-healable matrices, leading to heterogeneous crosslinked networks.[130-132] This strategy offers not only self-healable materials with high mechanical strength, but also provides extra functionalities such as sensing, energy storage and optical/electrical properties.[19] Compared to physical blending approach which involves bare CNTs embedded in polymeric matrix, our approach utilizes rMDBC/CNTs colloids, as multifunctional crosslinkers, through which CNTs are covalently embedded in self-healing matrix to promote their uniform distribution, thus enhancing conductivity and mechanical properties.

Polyurethane (PU) is an important class of industrial polymers and widely used in high-performance adhesives, surface coatings, surface sealants, foams, binder resins, sports devices, and electric products.[134] Recently, PU has been extensively utilized in the fabrication of self-healable materials through particularly Diels-Alder (DA) chemistry.[12, 49, 91]

This chapter describes the development of heterogeneous thermoreversible networks fabricated from a reactive mixture of a telechelic PU labeled with terminal furfuryl groups (Fu-PU), a bismaleimide (BM), and rMDBC/CNT colloids as a multiple crosslinker for macromolecular engineering approach based on DA/rDA chemistry. The partial cleavage of DA cycloadducts positioned on the backbone of the initially formed Fu-PU-BM linear copolymers could be favored for rDA reaction at elevated temperature. In turn, the cleaved products were recombined in the presence of furan-functionalized rMDBC/CNT multiple crosslinker under conditions favoring the DA reaction, resulting in the formation of a heterogeneous self-healable

network with uniformly distributed CNTs. The formed films were characterized for sol-gel transition, self-healing, and viscoelastic properties to demonstrate the versatility of the approach toward the development of multifunctional coating materials.

## 3.2 Experimental section

### 3.2.1 Materials

4,4′-Methylenebis(phenyl isocyanate) (MDI, 98%), polycaprolactone diol (PCL-DOH, average Mn ~2,000, 99.9%), dibutyltin dilaurate (DBTL, 95%), furfuryl alcohol (Fu-OH, 98%), and 1,1′-(methylenedi-4,1-phenylene) bismaleimide (BM, 95%) were purchased from Sigma-Aldrich and used as received.

### 3.2.2 Synthesis of a telechelic furan-terminated polyurethane (Fu-PU)

All the glassware was dried at 100 °C and cooled down to room temperature before polymerization. An organic solution of PCL-DOH (10.5 g, 5.3 mmol) and MDI (2.6 g, 10.6 mmol) dissolved in anhydrous THF (320 mL) was mixed with DBTDL (0.1% of PCL-DOH used) under nitrogen atmosphere at 60 °C for 3 hrs to synthesize polyurethane (PU) terminated with isocyanate. The addition of Fu-OH (1.0 g, 10.5 mmol) was followed for chain extension process and the resulting mixture was stirred for 5 hrs at 60 °C and then cooled down to room temperature to stop polymerization.

For structural characterization, an aliquot was precipitated from hexane and the precipitates were dried in a vacuum oven set at 50 °C.

### 3.2.3 Investigation of macromolecular engineering approach through sol-gel transition

Aliquots of the as-synthesized Fu-PU solution (10 g, solid content 8.7 %) was mixed with BM (0.2 g, 0.6 mmol) at 50 °C for 12 hrs to synthesize linear Fu-PU-BM copolymers with the mole equivalent ratio of furan/maleimide = 1/2. After the addition of rMDBC (0.5 g) dissolved in anisole (0.4 mL), the resulting mixture of Fu-PU-BM/rMDBC at 30 wt % was heated at 120 °C for 2 hrs. It was cooled down and kept at 50 °C for 2 hrs, forming a standing gel. It was again heated at 120 °C for 2 hrs, forming a sol, and cooled again and kept at 50 °C, reforming standing gel.

### 3.2.4 Fabrication of macromolecularly-engineered DA-crosslinked networks

A similar procedure was used to prepare a reactive mixture of Fu-PU-BM/rMDBC. Films were cast on a Teflon Petri dish and placed in a vacuum oven set at 50 °C for 3 days to fabricate macromolecularly-engineered DA-crosslinked network films.

### 3.2.5 Fabrication of heterogeneous DA-crosslinked networks covalently embedded with rMDBC/CNTs

Hybrid network was prepared by mixing MDBC (100 mg) and CNTs (10 mg) in anisole (5 mL). 0.1 %, 0.5 %, 1 % CNTs with respect to the weight (linear polymer + MDBC), were taken from the hybrid. After linear polymers were mixed with the aliquots in 120 ℃ oil bath for 2 hrs, the mixture was cast into a teflon petri dish and placed in 50 ℃ hot oven for 3 days to remove solvent.

### 3.2.6 Instrumentation and characterization

$^{1}$H-NMR spectra were recorded using a 500 MHz Varian spectrometer with $CDCl_3$ singlet at 7.26 ppm as the reference standard. Molecular weights of (co)polymers were analyzed by gel permeation chromatography (GPC). An Agilent GPC was equipped with a 1260 Infinity Isocratic Pump and a RI detector. Two Agilent PLgel mixed-C and mixed-D columns were used with DMF containing 0.1 mol% LiBr at 50 °C at a flow rate of 1.0 mL/min. Linear poly (methyl methacrylate) standards from Fluka were used for calibration. Aliquots of the polymer samples were dissolved in DMF/LiBr. The clear solutions were filtered using a 0.45 μm polytetrafluoroethylene (PTFE) filter to remove any DMF-insoluble species. A drop of anisole was added as a flow rate marker.

FT-IR spectra were recorded on a versatile Thermo Scientific TM iD5 ATR accessory for the Thermo Scientific TM Nicolet TM iS TM 5 FT-IR spectrometer, with 32 scans at room temperature in the range of 800 -2000 $cm^{-1}$.

Thermogravimetric analysis (TGA) was carried out using a TA instrument Q50 analyzer. Typically, dried samples were placed in a platinum pan inside a programmable furnace. They were then heated from 25 to 800 ℃ at a heating rate of 10 ℃/min under nitrogen flow. Mass loss was then calculated. Differential scanning calorimetry (DSC) analysis including glass transition temperature ($T_g$) of copolymers were measured with a TA Instruments DSC Q20 differential

scanning calorimeter. Samples were dried under vacuum for 24 hrs at room temperature to remove residual solvents. Temperature ranged from -80 to 200 ℃ for heating and cooking cycles conducted at a rate of 10 ℃/min. (Cycles: cool to from -80 ℃, heat up to 200 ℃ (1$^{st}$ run), cool to -80 ℃, heat up to 200 ℃ (2$^{nd}$ run), and cool to 25 ℃). The $T_g$ values were determined from the 2$^{nd}$ heating run.

Self-healing matrices were casted on glass plates at 50 °C and observed using an optical microscopy (Olympus BX51) with fluorescence filters (BP 460-490 excitation and BA520IF emission) coupled with a digital camera. Fresh cuts were made using a sharp blade on surfaces of the films at room temperature. They were placed in hot oven pre-set at 120 °C for 2 hrs, followed by 50 °C for 5 hrs. The samples cooled down to room temperature to investigate healing results.

Viscoelastic properties (G′ and G″ moduli) of self-healing matrices and self-healing composites were measured on DHT-2 rheometer (TA Instruments, USA) in frequency sweep mode, and amplitude strain shear mode with parallel plate geometry (8 mm diameter). For the frequency sweep mode, the gap was set to obtain an axial force around 5 N, and frequency was varied in the range of 1 rad/s and 100 rad/s. For the strain mode, the crosslinked materials were loaded on the plates and the % strain was varied in the range of 0.1 to 140% strain at 1 rad/s frequency. Lastly, cyclic changes of amplitude oscillatory from 5 % strain for 1500 s to 300 % strain for 500 s were tested. The gap was set to obtain an axial force of 5 N at room temperature.

### 3.3 Results and discussion

#### 3.3.1 Synthesis and characterization of rMDBC

Figure 3.1 depicts the chemical structure of a well-controlled rMDBC with narrow molecular weight distribution synthesized by a consecutive atom transfer radical polymerization (ATRP). The copolymer consists of a reactive poly(furfuryl methacrylate) (PFuMA) block and a anchoring polymethacrylate having pendant pyrene groups (PPyMA), thus forming PFuMA-b-PPyMA block copolymer. The copolymer had the number average molecular weight ($M_n$) = 19.5 kg/mol with dispersity as Đ <1.24 by GPC and the degree of polymerization (DP) = 27 for PFuMA block and 23 for PPyMA block by $^1$H-NMR spectroscopy. The detailed synthesis and characterization of rMDBC is reported in our previous publication.[135]

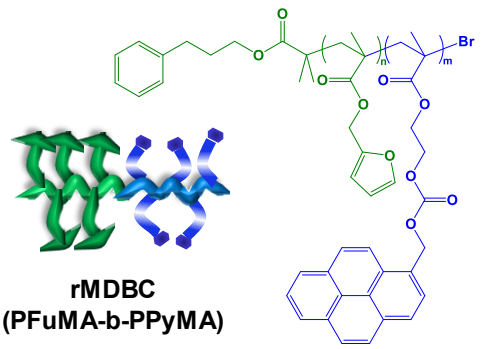


**Figure 3.1** Chemical structure of PFuMA-b- PPyMA (rMDBC) synthesized by a consecutive ATRP technique.

### 3.3.2 Synthesis and thermal analysis of telechelic Fu-PU by polyaddition

Figure 3.2 depicts our approach with two steps to synthesize a telechelic polyurethane functionalized with furfuryl groups at both chain ends (Fu-PU). The first step was the polyaddition of PCL-DOH to excess MDA in the presence of DBTL, a tin catalyst, at 60 °C. The mole equivalent ratio of OH/NCO was designed to be 1/2 to synthesize NCO-terminated PU precursors (PU). The PU content was set to be 5% in the recipe. Note that the formed PU solutions became viscous to gel when the PU content was designed with >15% in THF. After 3 hrs, the formed clear solution was determined to be 8.2% PU content by gravimetry. After purification by precipitation from hexane, the purified PU was characterized by $^{1}$H-NMR.

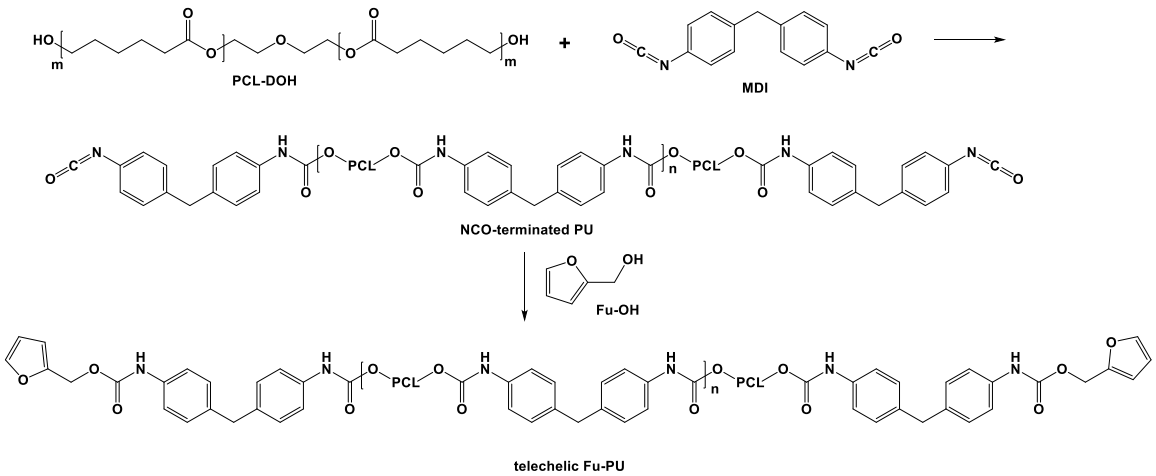


**Figure 3.2** Synthetic scheme of a telechelic polyurethane functionalized with terminal furfuryl groups (Fu-PU).

Figure 3.3 shows the presence of MDI units at 3.9 and 7.1 ppm and PCL units at 1.4, 1.7, 2.3, and 4.1 ppm, confirming the formation of PU (also see $^{1}$H-NMR spectra of PCL-DOH and MDI in Figure S3.1). The next step is the conjugation of the purified NCO-terminated PU with Fu-OH. The amount of Fu-OH was designed as the mole equivalent ratio of PCL-DOH/MDA/Fu-OH = 1/2/2, thus yielding a telechelic Fu-PU. The formed Fu-PU was subjected to extensive precipitation from hexane (three times) to remove unreacted (excess) Fu-OH. Note that hexane is a good solvent for furfuryl alcohol, but a poor solvent for FPU. The purified, dried Fu-PU was characterized by combined spectroscopic and thermal analysis. Its $^{1}$H-NMR spectrum shows the peaks correspond to furan ring protons at 6.4 and 7.4 ppm and methylene protons at 5.1 ppm (Figure 3.3).

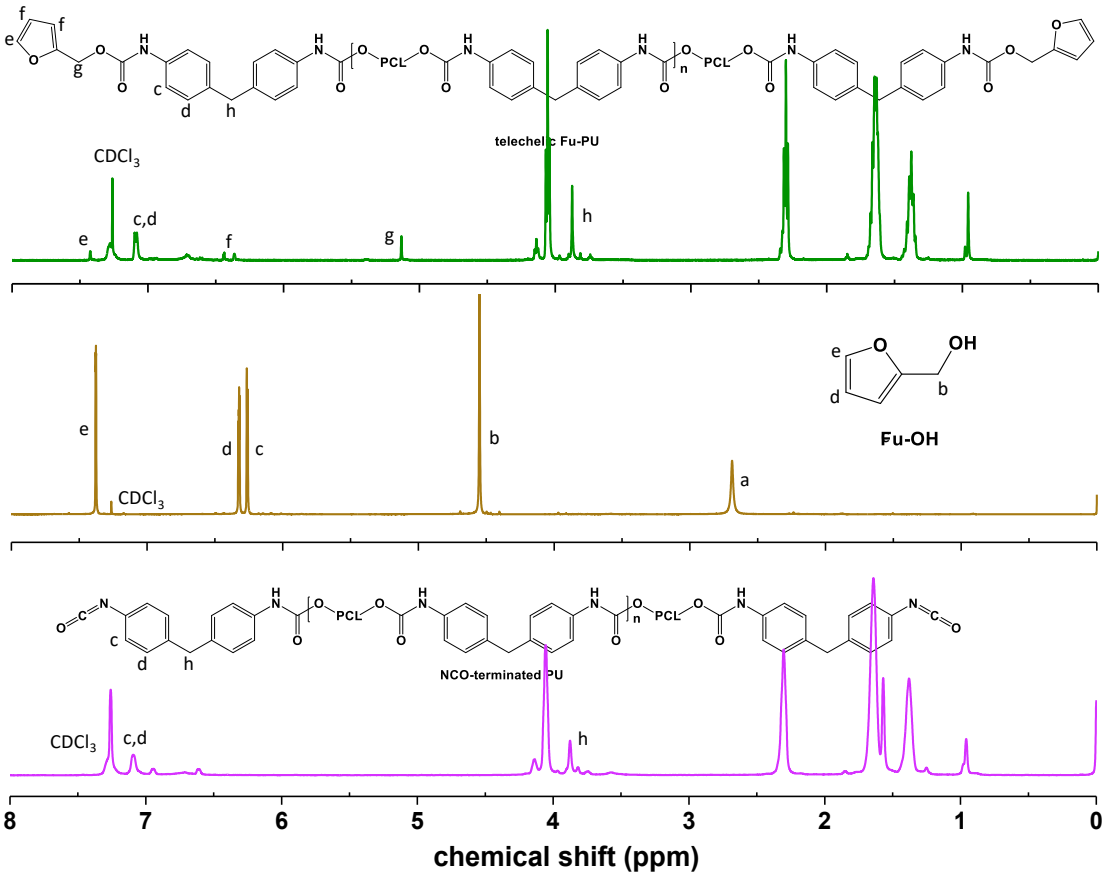


**Figure 3.3** $^{1}$H-NMR spectrum of Fu-PU, compared with those of its precursors PU and Fu-OH in $CDCl_3$.

FT-IR spectrum in Figure 3.4 shows a large carbonyl vibration at 1723 cm$^{-1}$ and a tiny furan vibration at 1012 cm$^{-1}$. GPC analysis confirms the molecular weight as the number average

molecular weight ($M_n$) = 10 kg/mol and $M_w/M_n$ = 1.6 (Figure S3.2). The Fu-PU was further characterized for thermal properties. DSC diagram in Figure S3.3 shows a glass transition at -43.7 °C and a sharp melting transition at 39 °C due to the crystalline PCL domains. These results obtained from our spectroscopic, DSC, and GPC analysis confirm the synthesis of telechelic Fu-PU.

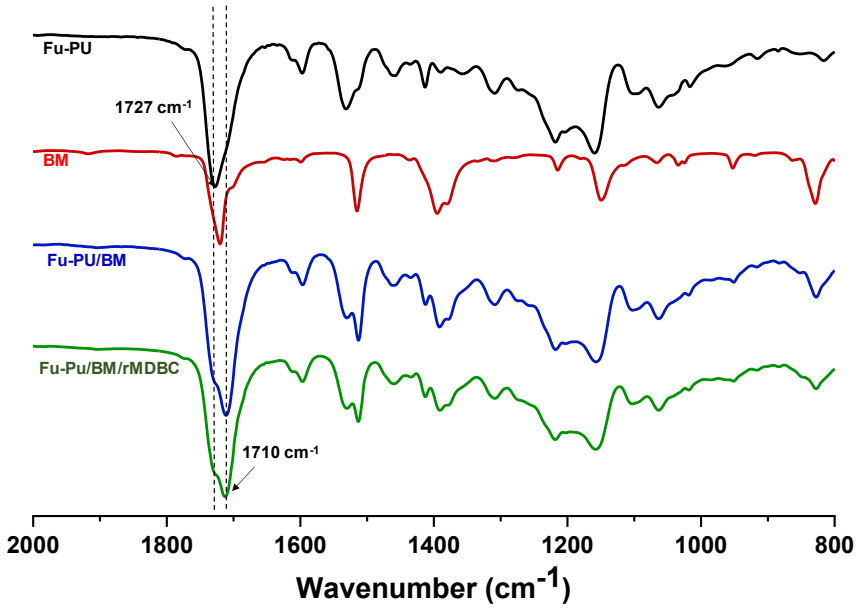


**Figure 3.4** FT-IR spectra of Fu-PU, BM, Fu-PU/BM linear polymer, and Fu-PU/BM/rMDBC film.

### 3.3.3 Investigation of macromolecular engineering approach with rMDBC as a multi-crosslinker

Macromolecular engineering approach through thermoreversibility was investigated with rMDBC having pendant furfuryl groups as a multi-crosslinker to form dynamic networks through DA/rDA reaction. As illustrated in Figure 3.5a, the first step was the polyaddition of difunctional Fu-PU with BM to synthesize linear Fu-PU-BM polymers through DA reaction at 60 °C in anisole. The polymerization was designed with the initial mole ratio of $[Fu\text{-}PU]_0/[BM]_0$ to be 1/2, which presents an excess of BM. The formed linear copolymer was characterized by FT-IR. As seen in Figure 3.4, the peak corresponding to carbonyl vibrations for the mixture of Fu-PU and BM is broad, with a new peak at 1710 $cm^{-1}$, which does not overlap with those corresponding to the carbonyl vibrations for its precursors, at 1727 $cm^{-1}$ for Fu-PU and 1720 $cm^{-}$

[1] for BM. As reported previously, such change is attributed to the occurrence of DA reaction of furfuryl groups with maleimide groups, yielding linear Fu-PU-BM copolymers.

The next step is the addition of rMDBC as a multiple crosslinker to the formed Fu-PU-BM copolymer in anisole to form macromolecularly-engineered network gels. The amount of rMDBC was designed to be 30/70 wt/wt of rMDBC/Fu-PU-BM. Thus, Fu-PU/BM/rMDBC = 55/15/30 wt/wt, equivalent to furan/maleimide/furan = 1/2/1. As seen in Figure 3.5b-3.5f, the reactive mixture was a homogeneous, transparent solution (b) and heated to 120 °C for 2 hrs to induce the occurrence of rDA reaction. The formed sol is the consequence of the dissociation of the mainchain DA bonds in Fu-PU-BM copolymers to mainly Fu-PU, BM, and Fu-PU-BM adducts at smaller molecular weight (c). Then, the sol cooled down to 60 °C and kept at the same temperature for 24 hrs to induce DA reaction of furan and maleimide groups, reforming a standing gel (d). Further, the standing gel was heated again to 120 °C for 2 hr to reform a sol (e), which was cooled and kept at 60 °C, re-yielding a standing gel (f). This process could be repeated many times through thermoreversibility of the DA-crosslinked networks.

Further, both linear Fu-PU-BM copolymer and gel were characterized by measuring relative heat flow with the temperature range at -80 - 200 ℃ by DSC. As seen in Figure S3.3, both, Fu-PU and Fu-PU-BM exhibit $T_g$ values of -40 and -35 °C respectively, but with no appearance of a melting transition which is shown in Fu-PU. The huge endotherm valley at 125 ℃ appeared in the 2$^{nd}$ heating run, which indicates the occurrence of the breaking of cleavage of DA-adducts through rDA reaction.

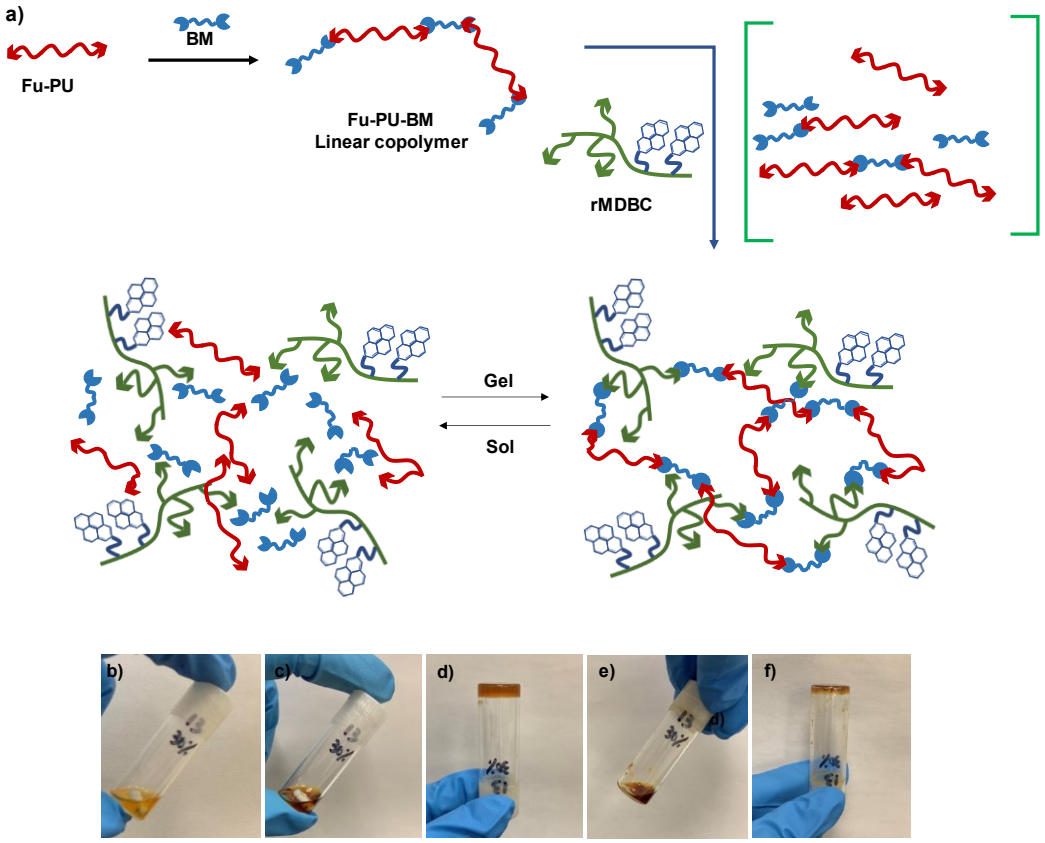


**Figure 3.5** Schematic illustration (a) and digital images (b-f) to show sol-gel transition for our macromolecular engineering approach through thermoreversibility of a reactive mixture consisting of Fu-PU, BM, and rMDBC in anisole at room temperature (b), heated at 120 °C for 2 hrs to sol (c), and cooled to and kept at 50 °C to reform standing gel (c), re-heated again to 120 °C for 2 hr to reform a sol (e), which was cooled and kept at 50 °C, re-yielding a standing gel (f). Condition for experiment: 30 wt% of solids consisting of rMDBC and Fu-PU-BM in anisole; Fu-PU/BM/rMDBC = 55/15/30 wt/wt.

### 3.3.4 Fabrication of DA-crosslinked networks

The crosslinked films fabricated with Fu-PU/BM/rMDBC = 55/15/30 wt% as above appeared to be too brittle to be further analyzed for their viscoelastic properties and self-healability. When the amount of rMDBC and BM were reduced to 5 wt% and 11 wt% separately, the flexible films were obtained, thus Fu-PU/BM/rMDBC = 84/11/5 wt/wt, equivalent to furan/maleimide/furan = 1/1/0.1 (Figure 3.6a). The formed films were characterized through frequency-sweep test using rheometer under the small amplitude oscillatory shear mode of the linear viscoelastic regime, to obtain viscoelastic properties. At the constant angular frequency of 10 rad/s, the storage modulus kept unchanged up to 1.5% strain; upon further increase in strain, it

rapidly decreased due to the rupture of the gel network (Figure 3.6b). In the range of angular frequency ranging from 0.1 to 100 rad/s and 5% strain, both G' and G'' kept significantly unchanged with slight increase of G′ (Figure 3.6c). Then, their self-healability was investigated using optical microscopy. Micron-sized cuts were made on the surface of the films by using a blade. They were placed in an oven pre-set at 120 ℃ for 2 hrs, promoting rDA reaction, and then at 50 ℃ for 2 hrs, allowing the re-establishment of DA linkages. Figure 3.6d-3.6e show the optical microscope images of the cuts before and after healing. Promisingly, the cut was completely healed through void-filling and following rDA/DA crosslinking.

These results from sol-gel experiment confirm the formation of dynamic networks with DA adducts through macromolecular engineering approach and thermoresponsive reversibility of the networks for robust self-healing.

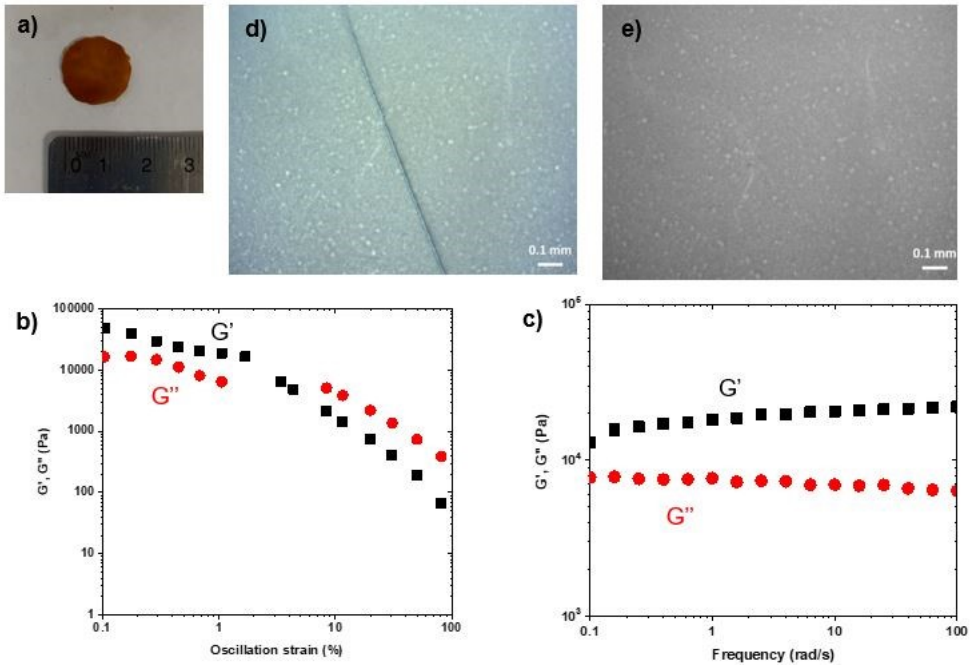


**Figure 3.6** Digital image of macromolecuarly-engineered film fabricated with Fu-PU/BM/rMDBC = 84/11/5 wt% (a); strain-sweep mode with strain ranging at 0.01 – 100% at angular frequency of 10 rad/s (b) and viscoelastic properties of G′ and G″ moduli through frequency-sweep mode with angular frequency ranging at 0.1 - 100 rad/s at 5% strain (c); and optical microscope images of a surface cut before (d) and after (e) being annealed at 120 °C for 2 hrs, followed by 50 °C for 12 hr. Inset in 6c: digital photo image of macromolecularly-engineered network gel.

### 3.3.5 Development of heterogeneous rMDBC/CNT-embedded DA-crosslinked networks

Given our promising results, similar procedure for macromolecular engineering approach was examined with rMDBC-stabilized CNTs to fabricated macromolecularly-engineered, heterogeneous, DA crosslinked networks covalently embedded with CNTs stabilized with rMDBC (Figure 3.7a). As a proof-of-concept, 0.5 wt% CNTs was added to the reactive mixture, attaining Fu-PU/BM/rMDBC/CNTs = 83.3/11.2/5/0.5 wt%. The mixture resulted in the formation of a standing gel through sol-gel transition shown in Figure 3.7b. In contrast, no standing gel was formed without rMDBC (Figure 3.7c). This result shows clear benefit for rMDBC strategy toward macromolecular engineering approach leading to heterogeneous network.

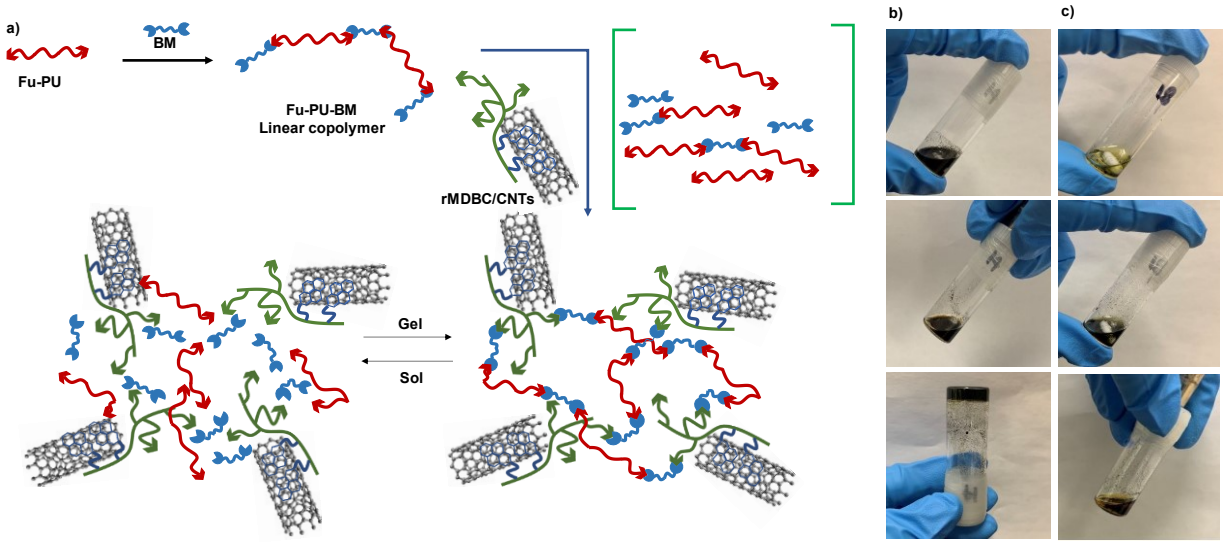


**Figure 3.7.** Schematic illustration to show our macromolecular engineering approach through thermoreversibility of a reactive mixture consisting of Fu-PU, BM, and CNTs with rMDBC (a). Digital images to show sol-gel transition with (b) and without (c) rMDBC in anisole at room temperature (upper), heated at 120 °C for 2 hrs to sol (middle), and cooled to and kept at 50 °C (lower). Condition for experiment: 30 wt% of solids consisting of Fu-PU/BM/rMDBC/CNTs = 83.3/11.2/5/0.5 wt% with rMDBC and Fu-PU-BM/CNTs = 99.5/0.5 wt% without rMDBC.

The formed films were found to be very flexible (Figure 3.8a). Their viscoelastic properties were analyzed with a cyclic change of oscillation force: 5% strain for 1500 sec to 95% strain for 500 sec under the constant 10 rad/s frequency. As seen in Figure 3.8b, the initial elastic modulus (G′) of the film was $6.5 \times 10^4$ Pa when a 5% strain was applied. Upon the change of oscillation

force to 95% strain, the G′ modulus dropped to <1000 Pa. Then, the G′ modulus was restored when the oscillation force was recovered back to 5% strain. Such a reversible restoration of G′ modulus was repeated several times, exhibiting self-healing elasticity of the crosslinked polymeric networks.

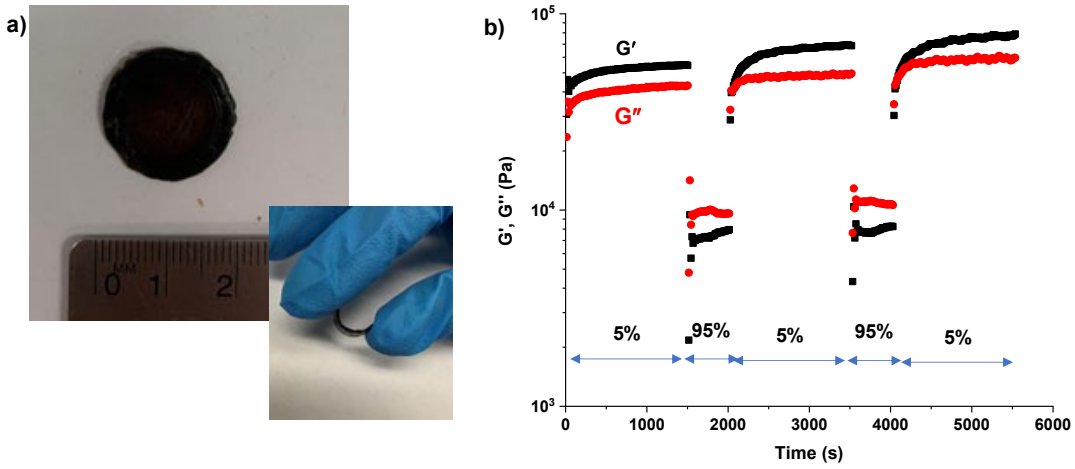


**Figure 3.8** Digital images of film cast from a reactive mixture of Fu-PU/BM/rMDBC/CNTs = 83.3/11.2/5/0.5 wt% (a) and viscoelastic properties using a rheometer upon a cyclic change of oscillation force: 5% strain for 1500 sec to 95% strain for 500 sec under the constant 10 rad/s frequency (b).

### 3.4 Conclusion

In conclusion, robust heterogeneous PU networks crosslinked with dynamic DA linkages and covalently embedded with CNTs stabilized with rMDBC were fabricated by macromolecular engineering approach through thermoreversibility based on DA/rDA chemistry utilizing rMDBC/CNT colloids as multiple crosslinkers. Linear copolymers bearing DA cycloadducts on the backbones were synthesized from a reactive mixture of a telechelic Fu-PU and BM. The control experiment through sol-gel transition reveals the use of rMDBC for the fabrication of heterogeneous PU networks. Promisingly, the fabricated PU network gels are flexible and robust to bent and exhibit self-healing elasticity. Furthermore significant characterizations, such as self-healing, recyclability, mechanical properties and conductivity, can be investigated to confirm the successful strategies of CNTs stabilization and fabrication of self-healing composite.

## 3.5 Supporting information

**Figure S3.1.** $^{1}$H-NMR spectra of PCL-DOH, MDI, and NCO-terminated PU in $CDCl_3$.

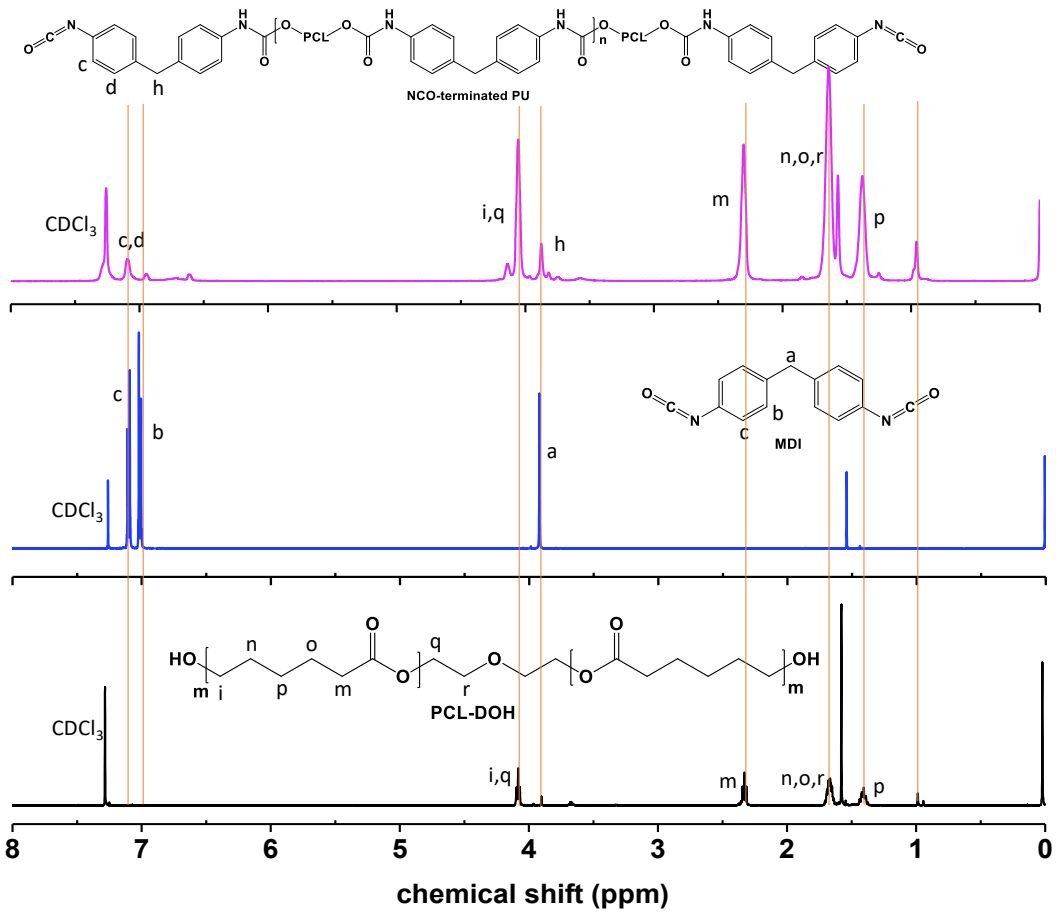

**Figure S3.2** GPC diagram of Fu-PU.

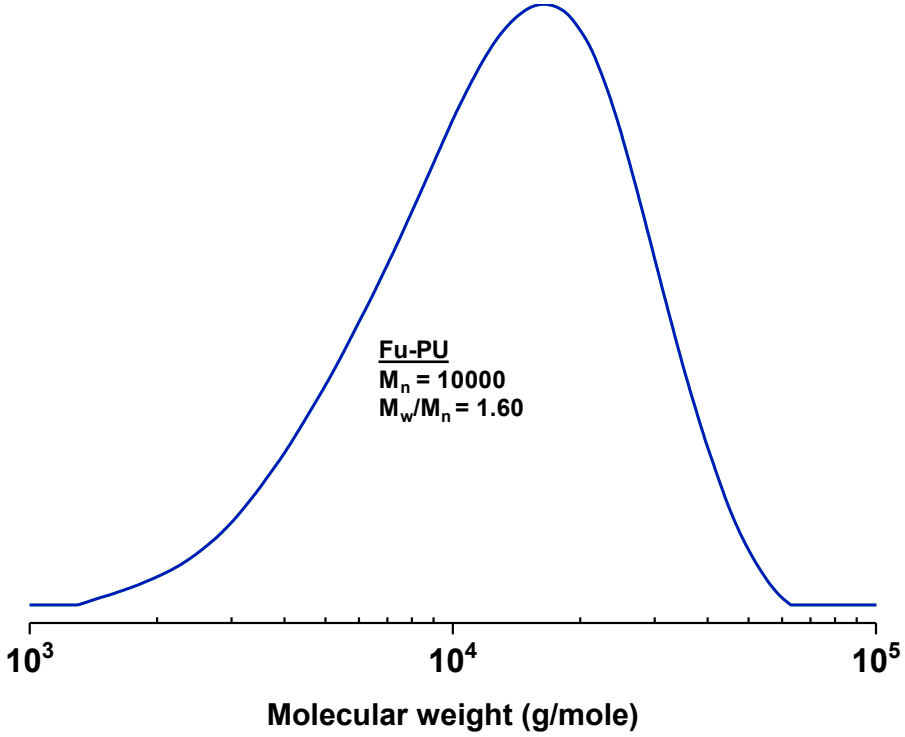


**Figure S3.3** DSC diagrams of Fu-PU, linear Fu-PU-BM copolymer, and macromolecularly-engineered Fu-PU-BM/rMDBC gel.

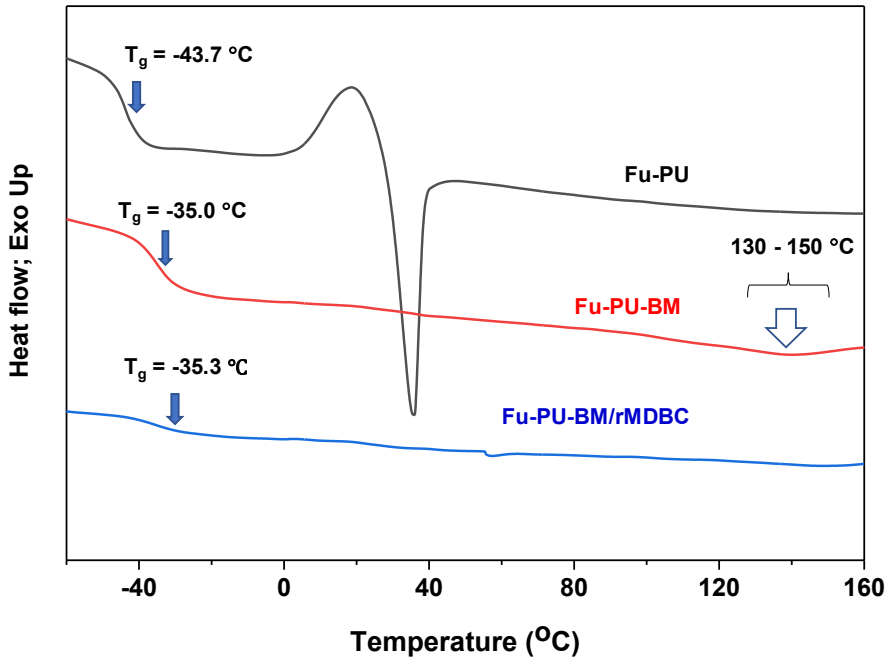

# Chapter 4
# Conclusion and Future Directions

My Masters' thesis research investigated a new platform for developing a robust heterogeneous thermoreversible networks with CNTs stabilized with covalentely incorporated rMDBC. Employing PU, having shape memory property and hydrogen bonding, the developed network materials exhibit robust self-healability and potentially enhanced mechanical property and conductivity.

Chapter 2 described our investigation of a new rMDBC stabilization strategy with the synthesis of a well-controlled PFuMA-b-PPyMA as an effective rMDBC having pendant furfuryl groups in one block and pyrene groups in the reactive block by consecutive ATRP technique. The synthesized rMDBC was effective in stabilizing CNT surfaces; thus its binding ability to CNTs was greater compared to the counterparts of homopolymer bearing pendant pyrene groups and a monodentate homopolymer labeled with a terminal pyrene group. The thermoreversible DA-crosslinked network with covalently embedded CNTs, exhibit thermoreversible self-healing through dynamic DA/rDA chemistry, confirmed by gel-sol-gel transition and thermal analysis. Chapter 3 summarized the development of robust heterogeneous PU networks crosslinked with dynamic DA linkages and covalently embedded CNTs, stabilized with rMDBC by macromolecular engineering approach utilizing rMDBC/CNT colloids as multiple crosslinkers. Our results confirmed that the fabricated PU network gels were flexible and robust to bend and exhibit excellent self-healing elasticity.

However, further studies are required to demonstrate the versatility of our approach to develop effective dynamic PU hybrid networks with uniform distribution of CNTs in DA-crosslinked films, which exhibite enhanced conductivity and mechanical properties. The amounts of CNTs in hybrid films will be varied to investigate their effect on self-healability, conductivity, and mechanical properties; thus optimal amount of CNTs will be determined for better performance. Further, the hybrid networks have to be examined for reprocessability and recyclability. Importantly, our robust approach can be applicable to other carbon materials such as graphene, carbon dots, and carbon quantum dots to demonstrate the applicability of our approach toward various applications in industries and materials science.

# References


1. Jud, K., H.H. Kausch, and J.G. Williams, *Fracture mechanics studies of crack healing and welding of polymers.* Journal of Materials Science, 1981. **16**(1): p. 204-210.
2. Malinskii, Y.M., et al., *Investigation of self-healing of cracks in polymers.* Polymer Mechanics, 1970. **6**(2): p. 240-244.
3. Nielsen, L.E., *Cross-Linking–Effect on Physical Properties of Polymers.* Journal of Macromolecular Science, Part C, 1969. **3**(1): p. 69-103.
4. Xing, X., et al., *A self-healing polymeric material: from gel to plastic.* Journal of Materials Chemistry A, 2014. **2**(29): p. 11049-11053.
5. Vatankhah-Varnoosfaderani, M., et al., *Rapid self-healing and triple stimuli responsiveness of a supramolecular polymer gel based on boron–catechol interactions in a novel water-soluble mussel-inspired copolymer.* Polymer Chemistry, 2014. **5**(2): p. 512-523.
6. An, S.Y., et al., *Recent strategies to develop self-healable crosslinked polymeric networks.* Chemical Communications, 2015. **51**(66): p. 13058-13070.
7. Wei, Z., et al., *Self-healing gels based on constitutional dynamic chemistry and their potential applications.* Chemical Society Reviews, 2014. **43**(23): p. 8114-8131.
8. Ji, S., et al., *Visible-Light-Induced Self-Healing Diselenide-Containing Polyurethane Elastomer.* Advanced Materials, 2015. **27**(47): p. 7740-7745.
9. Zhang, P., et al., *Redox- and pH-responsive polymer gels with reversible sol–gel transitions and self-healing properties.* RSC Advances, 2014. **4**(88): p. 47361-47367.
10. Hou, C., et al., *Bio-applicable and electroactive near-infrared laser-triggered self-healing hydrogels based on graphene networks.* Journal of Materials Chemistry, 2012. **22**(30): p. 14991-14996.
11. Jiang, Z.-C., et al., *Semi-IPNs with Moisture-Triggered Shape Memory and Self-Healing Properties.* Macromolecular Rapid Communications, 2017. **38**(14): p. 1700149.
12. Yang, L., et al., *Diels–Alder dynamic crosslinked polyurethane/polydopamine composites with NIR triggered self-healing function.* Polymer Chemistry, 2018. **9**(16): p. 2166-2172.
13. Fan, H., J. Wang, and Z. Jin, *Tough, Swelling-Resistant, Self-Healing, and Adhesive Dual-Cross-Linked Hydrogels Based on Polymer–Tannic Acid Multiple Hydrogen Bonds.* Macromolecules, 2018. **51**(5): p. 1696-1705.
14. Zhong, N. and W. Post, *Self-repair of structural and functional composites with intrinsically self-healing polymer matrices: A review.* Composites Part A: Applied Science and Manufacturing, 2015. **69**: p. 226-239.
15. An, S., et al., *A review on corrosion-protective extrinsic self-healing: Comparison of microcapsule-based systems and those based on core-shell vascular networks.* Chemical Engineering Journal, 2018. **344**: p. 206-220.
16. Zhou, S., H. Zhu, and Z. Yan, *Materials, Theories and Experiments of Microcapsule Self-Healing Method ? A Review.* Tunneling and Underground Construction: p. 195-204.
17. Lee, M.W., et al., *Advances in self-healing materials based on vascular networks with mechanical self-repair characteristics.* Advances in Colloid and Interface Science, 2018. **252**: p. 21-37.
18. Saba, N., et al., *A review on dynamic mechanical properties of natural fibre reinforced polymer composites.* Construction and Building Materials, 2016. **106**: p. 149-159.
19. Jouni, M., et al., *A representative and comprehensive review of the electrical and thermal properties of polymer composites with carbon nanotube and other nanoparticle fillers.* Polymer International, 2017. **66**(9): p. 1237-1251.
20. Zhang, Q., et al., *Review of recent achievements in self-healing conductive materials and their applications.* Journal of Materials Science, 2018. **53**(1): p. 27-46.

21. Gupta, M.K. and R.K. Srivastava, *Mechanical Properties of Hybrid Fibers-Reinforced Polymer Composite: A Review.* Polymer-Plastics Technology and Engineering, 2016. **55**(6): p. 626-642.
22. Amaral, A.J.R. and G. Pasparakis, *Stimuli responsive self-healing polymers: gels, elastomers and membranes.* Polymer Chemistry, 2017. **8**(42): p. 6464-6484.
23. Canadell, J., H. Goossens, and B. Klumperman, *Self-Healing Materials Based on Disulfide Links.* Macromolecules, 2011. **44**(8): p. 2536-2541.
24. Yoon, J.A., et al., *Self-Healing Polymer Films Based on Thiol–Disulfide Exchange Reactions and Self-Healing Kinetics Measured Using Atomic Force Microscopy.* Macromolecules, 2012. **45**(1): p. 142-149.
25. Zhao, D., et al., *UV Light Curable Self-Healing Superamphiphobic Coatings by Photopromoted Disulfide Exchange Reaction.* ACS Applied Polymer Materials, 2019. **1**(11): p. 2951-2960.
26. An, S.Y., et al., *Dual Sulfide–Disulfide Crosslinked Networks with Rapid and Room Temperature Self-Healability.* Macromolecular Rapid Communications, 2015. **36**(13): p. 1255-1260.
27. An, S.Y., S.M. Noh, and J.K. Oh, *Multiblock Copolymer-Based Dual Dynamic Disulfide and Supramolecular Crosslinked Self-Healing Networks.* Macromolecular Rapid Communications, 2017. **38**(8): p. 1600777.
28. Tasdelen, M.A., *Diels-Alder "click" reactions: recent applications in polymer and material science.* Polym. Chem., 2011. **2**(10): p. 2133-2145.
29. Jung, S., T. Patel, and J.K. Oh, *Thermally Labile Self-Healable Branched Gel Networks Fabricated by New Macromolecular Engineering Approach Utilizing Thermoreversibility.* Macromolecular Rapid Communications, 2018. **39**(5): p. 1700575.
30. Berto, P., et al., *Recyclable Telechelic Cross-Linked Polybutadiene Based on Reversible Diels–Alder Chemistry.* Macromolecules, 2018. **51**(3): p. 651-659.
31. Jung, S., et al., *A new reactive polymethacrylate bearing pendant furfuryl groups: Synthesis, thermoreversible reactions, and self-healing.* Polymer, 2017. **109**: p. 58-65.
32. Arunbabu, D., et al., *Thermoreversible Self-Healing Networks Based on a Tunable Polymethacrylate Crossslinker Having Pendant Maleimide Groups.* Macromol. Chem. Phys., 2016. **217**(19): p. 2191-2198.
33. Jung, S., et al., *Ambient temperature induced Diels-Alder crosslinked networks based on controlled methacrylate copolymers for enhanced thermoreversibility and self-healability.* RSC Adv., 2017. **7**(42): p. 26496-26506.
34. Jung, S. and J.K. Oh, *Well-defined methacrylate copolymer having reactive maleimide pendants for fabrication of thermally-labile crosslinked networks with robust self-healing.* Mater. Today Commun., 2017. **13**: p. 241-247.
35. Ying, H., et al., *Hindered Urea Bond: A Bilaterally Responsive Chemistry to Hydrogen Peroxide.* European Journal of Organic Chemistry, 2019. **2019**(4): p. 728-731.
36. Jiang, L., et al., *Sustainable Thermosetting Polyurea Vitrimers Based on a Catalyst-Free Process with Reprocessability, Permanent Shape Reconfiguration and Self-Healing Performance.* ACS Applied Polymer Materials, 2019. **1**(12): p. 3261-3268.
37. Chao, A., I. Negulescu, and D. Zhang, *Dynamic Covalent Polymer Networks Based on Degenerative Imine Bond Exchange: Tuning the Malleability and Self-Healing Properties by Solvent.* Macromolecules, 2016. **49**(17): p. 6277-6284.
38. Han, X., et al., *Dynamic imine bond cross-linked self-healing thermosensitive hydrogels for sustained anticancer therapy via intratumoral injection.* Materials Science and Engineering: C, 2018. **93**: p. 1064-1072.
39. Kuhl, N., et al., *Acylhydrazones as Reversible Covalent Crosslinkers for Self-Healing Polymers.* Advanced Functional Materials, 2015. **25**(22): p. 3295-3301.

40. Lu, Y.-X. and Z. Guan, *Olefin Metathesis for Effective Polymer Healing via Dynamic Exchange of Strong Carbon–Carbon Double Bonds.* Journal of the American Chemical Society, 2012. **134**(34): p. 14226-14231.
41. Cromwell, O.R., J. Chung, and Z. Guan, *Malleable and Self-Healing Covalent Polymer Networks through Tunable Dynamic Boronic Ester Bonds.* Journal of the American Chemical Society, 2015. **137**(20): p. 6492-6495.
42. Ling, J., M.Z. Rong, and M.Q. Zhang, *Photo-stimulated self-healing polyurethane containing dihydroxyl coumarin derivatives.* Polymer, 2012. **53**(13): p. 2691-2698.
43. Herbst, F., et al., *Self-Healing Polymers via Supramolecular Forces.* Macromolecular Rapid Communications, 2013. **34**(3): p. 203-220.
44. van Gemert, G.M.L., et al., *Self-Healing Supramolecular Polymers In Action.* Macromolecular Chemistry and Physics, 2012. **213**(2): p. 234-242.
45. Shao, C., et al., *High-Strength, Tough, and Self-Healing Nanocomposite Physical Hydrogels Based on the Synergistic Effects of Dynamic Hydrogen Bond and Dual Coordination Bonds.* ACS Applied Materials & Interfaces, 2017. **9**(34): p. 28305-28318.
46. Zhang, H., H. Xia, and Y. Zhao, *Poly(vinyl alcohol) Hydrogel Can Autonomously Self-Heal.* ACS Macro Letters, 2012. **1**(11): p. 1233-1236.
47. Cui, X., et al., *Self-healing polymers with tunable mechanical strengths via combined hydrogen bonding and zinc-imidazole interactions.* Polymer, 2019. **174**: p. 143-149.
48. Jian, X., et al., *Self-healing polyurethane based on disulfide bond and hydrogen bond.* Polymers for Advanced Technologies, 2018. **29**(1): p. 463-469.
49. Rivero, G., et al., *One-Pot Thermo-Remendable Shape Memory Polyurethanes.* Macromolecules, 2014. **47**(6): p. 2010-2018.
50. Burattini, S., et al., *A Healable Supramolecular Polymer Blend Based on Aromatic π–π Stacking and Hydrogen-Bonding Interactions.* Journal of the American Chemical Society, 2010. **132**(34): p. 12051-12058.
51. Fox, J., et al., *High-Strength, Healable, Supramolecular Polymer Nanocomposites.* Journal of the American Chemical Society, 2012. **134**(11): p. 5362-5368.
52. Bose, R.K., et al., *Connecting supramolecular bond lifetime and network mobility for scratch healing in poly(butyl acrylate) ionomers containing sodium, zinc and cobalt.* Physical Chemistry Chemical Physics, 2015. **17**(3): p. 1697-1704.
53. Huang, Y., P.G. Lawrence, and Y. Lapitsky, *Self-Assembly of Stiff, Adhesive and Self-Healing Gels from Common Polyelectrolytes.* Langmuir, 2014. **30**(26): p. 7771-7777.
54. Wei, Z., et al., *Autonomous self-healing of poly(acrylic acid) hydrogels induced by the migration of ferric ions.* Polymer Chemistry, 2013. **4**(17): p. 4601-4605.
55. Darabi, M.A., et al., *Skin-Inspired Multifunctional Autonomic-Intrinsic Conductive Self-Healing Hydrogels with Pressure Sensitivity, Stretchability, and 3D Printability.* Advanced Materials, 2017. **29**(31): p. 1700533.
56. Cao, Y., et al., *A Transparent, Self-Healing, Highly Stretchable Ionic Conductor.* Advanced Materials, 2017. **29**(10): p. 1605099.
57. Wang, W., R. Narain, and H. Zeng, *Rational Design of Self-Healing Tough Hydrogels: A Mini Review.* Frontiers in Chemistry, 2018. **6**: p. 497.
58. Loh, X.J., *Supramolecular host–guest polymeric materials for biomedical applications.* Materials Horizons, 2014. **1**(2): p. 185-195.
59. Hu, Z., et al., *Multistimuli-Responsive Intrinsic Self-Healing Epoxy Resin Constructed by Host–Guest Interactions.* Macromolecules, 2018. **51**(14): p. 5294-5303.
60. Li, C.-H., et al., *A highly stretchable autonomous self-healing elastomer.* Nature Chemistry, 2016. **8**(6): p. 618-624.

61. Zheng, Q., Z. Ma, and S. Gong, *Multi-stimuli-responsive self-healing metallo-supramolecular polymer nanocomposites.* Journal of Materials Chemistry A, 2016. **4**(9): p. 3324-3334.
62. Zhao, Y., et al., *Encapsulation of Self-Healing Agents in Polymer Nanocapsules.* Small, 2012. **8**(19): p. 2954-2958.
63. Samadzadeh, M., et al., *A review on self-healing coatings based on micro/nanocapsules.* Progress in Organic Coatings, 2010. **68**(3): p. 159-164.
64. White, S.R., et al., *Autonomic healing of polymer composites.* Nature, 2001. **409**(6822): p. 794-797.
65. Keller, M.W., S.R. White, and N.R. Sottos, *A Self-Healing Poly(Dimethyl Siloxane) Elastomer.* Advanced Functional Materials, 2007. **17**(14): p. 2399-2404.
66. Caruso, M.M., et al., *Solvent-Promoted Self-Healing Epoxy Materials.* Macromolecules, 2007. **40**(25): p. 8830-8832.
67. Salvetat, J.P., et al., *Mechanical properties of carbon nanotubes.* Applied Physics A, 1999. **69**(3): p. 255-260.
68. Ebbesen, T.W., et al., *Electrical conductivity of individual carbon nanotubes.* Nature, 1996. **382**(6586): p. 54-56.
69. Qian, D., et al., *Mechanics of carbon nanotubes.* Applied Mechanics Reviews, 2002. **55**(6): p. 495-533.
70. Han, Z. and A. Fina, *Thermal conductivity of carbon nanotubes and their polymer nanocomposites: A review.* Progress in Polymer Science, 2011. **36**(7): p. 914-944.
71. Parveen, S., S. Rana, and R. Fangueiro, *A Review on Nanomaterial Dispersion, Microstructure, and Mechanical Properties of Carbon Nanotube and Nanofiber Reinforced Cementitious Composites.* Journal of Nanomaterials, 2013. **2013**: p. 710175.
72. Huang, Y.Y. and E.M. Terentjev, *Dispersion of Carbon Nanotubes: Mixing, Sonication, Stabilization, and Composite Properties.* Polymers, 2012. **4**(1).
73. Vander Wal, R.L., et al., *Friction properties of surface-fluorinated carbon nanotubes.* Wear, 2005. **259**(1): p. 738-743.
74. Vast, L., et al., *Chemical functionalization by a fluorinated trichlorosilane of multi-walled carbon nanotubes.* Nanotechnology, 2004. **15**(7): p. 781-785.
75. Lu, X., et al., *A Theoretical Exploration of the 1,3-Dipolar Cycloadditions onto the Sidewalls of (n,n) Armchair Single-Wall Carbon Nanotubes.* Journal of the American Chemical Society, 2003. **125**(34): p. 10459-10464.
76. Pekker, S., et al., *Hydrogenation of Carbon Nanotubes and Graphite in Liquid Ammonia.* The Journal of Physical Chemistry B, 2001. **105**(33): p. 7938-7943.
77. Wu, H.-X., et al., *Functionalization of multiwalled carbon nanotubes with polystyrene under atom transfer radical polymerization conditions.* Carbon, 2007. **45**(1): p. 152-159.
78. Zhang, J., et al., *Effect of Chemical Oxidation on the Structure of Single-Walled Carbon Nanotubes.* The Journal of Physical Chemistry B, 2003. **107**(16): p. 3712-3718.
79. Wu, G., et al., *Interface enhancement of carbon fiber reinforced methylphenylsilicone resin composites modified with silanized carbon nanotubes.* Materials & Design, 2016. **89**: p. 1343-1349.
80. Homenick, C.M., G. Lawson, and A. Adronov, *Polymer Grafting of Carbon Nanotubes Using Living Free‐Radical Polymerization.* Polymer Reviews, 2007. **47**(2): p. 265-290.
81. Liu, W., et al., *Interactions between Single-Walled Carbon Nanotubes and Polyethylene/Polypropylene/Polystyrene/Poly(phenylacetylene)/Poly(p-phenylenevinylene) Considering Repeat Unit Arrangements and Conformations: A Molecular Dynamics Simulation Study.* The Journal of Physical Chemistry C, 2008. **112**(6): p. 1803-1811.

82. Vo, M.D., et al., *Adsorption of anionic and non-ionic surfactants on carbon nanotubes in water with dissipative particle dynamics simulation.* The Journal of Chemical Physics, 2016. **144**(20): p. 204701.
83. Khlobystov, A.N., et al., *Molecular Motion of Endohedral Fullerenes in Single-Walled Carbon Nanotubes.* Angewandte Chemie International Edition, 2004. **43**(11): p. 1386-1389.
84. Ma, P.-C., et al., *Dispersion and functionalization of carbon nanotubes for polymer-based nanocomposites: A review.* Composites Part A: Applied Science and Manufacturing, 2010. **41**(10): p. 1345-1367.
85. Pérez-Madrigal, M.M., et al., *Electronic, electric and electrochemical properties of bioactive nanomembranes made of polythiophene:thermoplastic polyurethane.* Polymer Chemistry, 2014. **5**(4): p. 1248-1257.
86. Pan, H., et al., *Fabrication of binary hybrid-filled layer-by-layer coatings on flexible polyurethane foams and studies on their flame-retardant and thermal properties.* RSC Advances, 2016. **6**(82): p. 78286-78295.
87. Kirpluks, M., et al., *Natural oil based highly functional polyols as feedstock for rigid polyurethane foam thermal insulation.* Industrial Crops and Products, 2018. **122**: p. 627-636.
88. Filip, D., et al., *Surface characterization and antimicrobial properties of sodium deoxycholate-based poly(ester ether)urethane ionomer biomaterials.* Reactive and Functional Polymers, 2016. **102**: p. 70-81.
89. Feng, L., et al., *Self-healing behavior of polyurethanes based on dual actions of thermo-reversible Diels-Alder reaction and thermal movement of molecular chains.* Polymer, 2017. **124**: p. 48-59.
90. Huang, J., et al. *Dielectric self-healing BNNS/PU nanocomposites based on DA chemistry*. in *2019 20th International Conference on Electronic Packaging Technology(ICEPT)*. 2019.
91. Fu, G., et al., *Heat-resistant polyurethane films with great electrostatic dissipation capacity and very high thermally reversible self-healing efficiency based on multi-furan and liquid multi-maleimide polymers.* Journal of Materials Chemistry A, 2016. **4**(11): p. 4232-4241.
92. Fang, Y., et al., *Thermal- and mechanical-responsive polyurethane elastomers with self-healing, mechanical-reinforced, and thermal-stable capabilities.* Polymer, 2018. **158**: p. 166-175.
93. Fang, Y., et al., *Preparation of living and highly stable blended polyurethane emulsions for self-healing films with enhancive toughness and recyclability.* Polymer, 2020. **188**: p. 122142.
94. Chang, K., H. Jia, and S.-Y. Gu, *A transparent, highly stretchable, self-healing polyurethane based on disulfide bonds.* European Polymer Journal, 2019. **112**: p. 822-831.
95. Cushing, B.L., V.L. Kolesnichenko, and C.J. O'Connor, *Recent Advances in the Liquid-Phase Syntheses of Inorganic Nanoparticles.* Chem. Rev., 2004. **104**(9): p. 3893-3946.
96. Bruchez, M., Jr., et al., *Semiconductor nanocrystals as fluorescent biological labels.* Science, 1998. **281**(5385): p. 2013-2016.
97. Somers, R.C., M.G. Bawendi, and D.G. Nocera, *CdSe nanocrystal based chem-/bio- sensors.* Chem. Soc. Rev., 2007. **36**(4): p. 579-591.
98. Wu, Z.L., Z.X. Liu, and Y.H. Yuan, *Carbon dots: materials, synthesis, properties and approaches to long-wavelength and multicolor emission.* J. Mater. Chem. B, 2017. **5**(21): p. 3794-3809.
99. Sivakumar, P., et al., *Photo-triggered antibacterial and anticancer activities of zinc oxide nanoparticles.* J. Mater. Chem. B, 2018. **6**(30): p. 4852-4871.
100. Pelaz, B., et al., *Diverse Applications of Nanomedicine.* ACS Nano, 2017. **11**(3): p. 2313-2381.
101. Baughman, R.H., A.A. Zakhidov, and W.A. de Heer, *Carbon nanotubes-the route toward applications.* Science 2002. **297**(5582): p. 787-792.
102. Oh, J.K. and J.M. Park, *Iron oxide-based superparamagnetic polymeric nanomaterials: Design, preparation, and biomedical application.* Prog. Polym. Sci., 2011. **36**(1): p. 168-189.

103. Oh, J.K., *Surface modification of colloidal CdX-based quantum dots for biomedical applications.* J. Mater. Chem., 2010. **20**(39): p. 8433-8445.
104. Zhang, Y., C.T. Supuran, and M. Barboiu, *Exponential Activation of Carbonic Anhydrase by Encapsulation in Dynameric Host Matrices with Chiral Discrimination.* Chem. - Eur. J., 2018. **24**(3): p. 715-720.
105. Zhang, Y., et al., *Dynamic encapsulation and activation of carbonic anhydrase in multivalent dynameric host matrices.* Chem. Commun. , 2016. **52**(21): p. 4053-4055.
106. Na, H.B., et al., *Multidentate Catechol-Based Polyethylene Glycol Oligomers Provide Enhanced Stability and Biocompatibility to Iron Oxide Nanoparticles.* ACS Nano, 2012. **6**(1): p. 389-399.
107. Fokina, A., et al., *Multidentate Polysarcosine-Based Ligands for Water-Soluble Quantum Dots.* Macromolecules (Washington, DC, U. S.), 2016. **49**(10): p. 3663-3671.
108. Chan, N., et al., *Multidentate Block-Copolymer-Stabilized Ultrasmall Superparamagnetic Iron Oxide Nanoparticles with Enhanced Colloidal Stability for Magnetic Resonance Imaging.* Biomacromolecules, 2014. **15**(6): p. 2146-2156.
109. Li, P., et al., *Mussel-Inspired Multidentate Block Copolymer to Stabilize Ultrasmall Superparamagnetic Fe3O4 for Magnetic Resonance Imaging Contrast Enhancement and Excellent Colloidal Stability.* Chem. Mater., 2015. **27**(20): p. 7100-7109.
110. Xiao, W., et al., *Superparamagnetic Iron Oxide Nanoparticles Stabilized with Multidentate Block Copolymers for Optimal Vascular Contrast in T1-Weighted Magnetic Resonance Imaging.* ACS Appl. Nano Mater., 2018. **1**(2): p. 894-907.
111. Wang, M., et al., *Colloidal CdSe nanocrystals passivated by a dye-labeled multidentate polymer: quantitative analysis by size-exclusion chromatography.* Angew. Chem., Int. Ed., 2006. **45**(14): p. 2221-2224.
112. Ma, L., et al., *Multidentate Polymer Coatings for Compact and Homogeneous Quantum Dots with Efficient Bioconjugation.* J. Am. Chem. Soc., 2016. **138**(10): p. 3382-3394.
113. Zheng, Z., et al., *Luminescent zinc oxide nanoparticles: from stabilization to slow digestion depending on the nature of polymer coating.* Polym. Chem., 2019. **10**(1): p. 145-154.
114. Kloxin, C.J. and C.N. Bowman, *Covalent adaptable networks: smart, reconfigurable and responsive network systems.* Chem. Soc. Rev., 2013. **42**(17): p. 7161-7173.
115. Denissen, W., J.M. Winne, and F.E. Du Prez, *Vitrimers: permanent organic networks with glass-like fluidity.* Chem. Sci., 2016. **7**(1): p. 30-38.
116. Montarnal, D., et al., *Silica-Like Malleable Materials from Permanent Organic Networks.* Science (Washington, DC, U. S.), 2011. **334**(6058): p. 965-968.
117. Chen, X., et al., *A thermally re-mendable cross-linked polymeric material.* Science, 2002. **295**(5560): p. 1698-702.
118. Jung, S., T. Patel, and J.K. Oh, *Thermally Labile Self-Healable Branched Gel Networks Fabricated by New Macromolecular Engineering Approach Utilizing Thermoreversibility.* Macromol. Rapid Commun., 2018. **39**(5): p. 1700575.
119. Lyon, G.B., A. Baranek, and C.N. Bowman, *Scaffolded Thermally Remendable Hybrid Polymer Networks.* Adv. Funct. Mater., 2016. **26**(9): p. 1477-1485.
120. An, S.Y., S. Sun, and J.K. Oh, *Reduction-Responsive Sheddable Carbon Nanotubes Dispersed in Aqueous Solution.* Macromol. Rapid Commun., 2016. **37**(8): p. 705-710.
121. Yuan, W.Z., et al., *Wrapping carbon nanotubes in pyrene-containing poly(phenylacetylene) chains: solubility, stability, light emission, and surface photovoltaic properties.* Macromolecules, 2006. **39**: p. 8011-8020.
122. Meuer, S., L. Braun, and R. Zentel, *Solubilisation of multi walled carbon nanotubes by alpha-pyrene functionalised PMMA and their liquid crystalline self-organisation.* Chem. Commun., 2008(27): p. 3166-8.

123. Coleman, J.N., et al., *Small but strong: A review of the mechanical properties of carbon nanotube–polymer composites.* Carbon, 2006. **44**(9): p. 1624-1652.
124. Taft, B.J., et al., *Site-specific assembly of DNA and appended cargo on arrayed carbon nanotubes.* J. Am. Chem. Soc., 2004. **126**: p. 12750-12751.
125. Ramesh, P., et al., *SWNT-MWCT hybrid architecture for proton exchange membrane fuel cell cathodes.* J. Phys. Chem. C, 2008. **112**: p. 9089-9094.
126. Liu, Z., et al., *Supramolecular chmistry on water-soluble carbon nanotubes for drug loading and delivery.* ACS Nano, 2007. **1**: p. 50-56.
127. Matyjaszewski, K. and J. Xia, *Atom Transfer Radical Polymerization.* Chem. Rev. , 2001. **101**(9): p. 2921-2990.
128. Kamigaito, M., T. Ando, and M. Sawamoto, *Metal-Catalyzed Living Radical Polymerization.* Chem. Rev. , 2001. **101**(12): p. 3689-3745.
129. Kavitha, A.A. and N.K. Singha, *Smart "All Acrylate" ABA Triblock Copolymer Bearing Reactive Functionality via Atom Transfer Radical Polymerization (ATRP): Demonstration of a "Click Reaction" in Thermoreversible Property.* Macromolecules 2010. **43**(7): p. 3193-3205.
130. Guimard, N.K., et al., *Current Trends in the Field of Self-Healing Materials.* Macromolecular Chemistry and Physics, 2012. **213**(2): p. 131-143.
131. Ramesh, M., et al., *22 - Self-healing polymer composites and its chemistry*, in *Self-Healing Composite Materials*, A. Khan, et al., Editors. 2020, Woodhead Publishing. p. 415-427.
132. Thakur, V.K. and M.R. Kessler, *Self-healing polymer nanocomposite materials: A review.* Polymer, 2015. **69**: p. 369-383.
133. Xie, X.-L., Y.-W. Mai, and X.-P. Zhou, *Dispersion and alignment of carbon nanotubes in polymer matrix: A review.* Materials Science and Engineering: R: Reports, 2005. **49**(4): p. 89-112.
134. Akindoyo, J.O., et al., *Polyurethane types, synthesis and applications – a review.* RSC Advances, 2016. **6**(115): p. 114453-114482.
135. Zhang, G. and J.K. Oh, *Reactive Multidentate Block Copolymer Stabilization to Carbon Nanotubes for Thermoreversible Cross-Linked Network Gels.* ACS Appl. Polym. Mater., 2020: p. Ahead of Print.